

Recent advances in graphene aerogels as absorption-dominated electromagnetic interference shielding materials

Zheng Cheng^{a,1}, Ruofeng Wang^{a,1}, Yang Wang^a, Yishu Cao^a, Yuxiang Shen^a, Yi Huang^{a,*}, Yongsheng Chen^{b,**}

^a National Institute for Advanced Materials, Key Laboratory of Functional Polymer Materials, School of Materials Science and Engineering, Nankai University, Tianjin, 300350, PR China

^b Key Laboratory of Functional Polymer Materials, State Key Laboratory and Institute of Elemento-Organic Chemistry, Centre for Nanoscale Science and Technology, Institute of Polymer Chemistry, College of Chemistry, Nankai University, Tianjin, 300350, PR China

ARTICLE INFO

Keywords:

Graphene aerogel
EMI shielding
Microwave absorption
Structural design
Smart and multi-functional materials

ABSTRACT

The design of lightweight and efficient electromagnetic interference (EMI) shielding materials is of great importance in both civil and military fields. Recently, graphene aerogels with three-dimensional structure have been proven to be efficient EMI shielding materials with superior advantages of low density, strong absorption of microwaves, and multi-band applicability. More importantly, most graphene aerogels and their composites exhibit the absorption-dominated shielding performance, which is exactly the future developing trend for EMI shielding materials. In this review, we summarized the recent progresses of graphene aerogel-based EMI shielding materials. Firstly, the key concepts, mechanisms of EMI shielding, and the advantages of graphene aerogels as EMI shielding materials are discussed in detail. Then, the fabrication strategies of graphene aerogels are summarized, and their advantages and disadvantages are both narrated. Thirdly, various kinds of graphene aerogels and their composites are reviewed, with their overall structure-function relationship and absorption-dominated shielding mechanism illustrated. Fourthly, smart and multi-functional graphene aerogels as EMI shielding materials are also discussed. Finally, the challenges and technical problems are proposed, and development trends are prospected.

1. Introduction

The rapid development of electromagnetic (EM) wave technology has greatly promoted the development of the society. Numerous technologies based on the EM waves, such as the fifth-generation (5G) communication and radar detection have significantly changed people's lives [1,2]. Nevertheless, problems are also arising during the application of EM wave technology. In the civil fields, electromagnetic interference and leakage always exist, and these have caused bad influences on the instant messaging and networking. Moreover, it has been reported that strong electromagnetic radiation will produce deleterious effects on human body, particularly the nervous system. Some symptoms caused by the EM wave pollution, including anxiety, headaches, depression have been reported [3,4]. While in the military fields, high-energy electromagnetic weapons are being developed by several

countries, which poses a huge threat to the high-value equipment, such as satellites, computer network and electrical power systems. Therefore, electromagnetic interference (EMI) shielding materials are becoming more and more important in recent years, which could prevent electromagnetic leakage to ensure the safety of electronic communication, and protect important military installations and people's health [5–8].

EMI shielding materials are functional materials that can shield EM waves by blocking or attenuating them. For practical applications, EMI shielding materials are generally placed on the surface of equipment, serving as a barrier for incident or leaked EM waves. Electromagnetic interference shielding effectiveness (EMI SE) is usually used to quantitatively evaluate the shielding effects of EMI shielding materials in decibel (dB). The EMI SE value is relevant to several aspects, including electromagnetic properties and thickness of the materials, the EM wave frequency, and the distance between the interference source and the

* Corresponding author.

** Corresponding author.

E-mail addresses: yihuang@nankai.edu.cn (Y. Huang), yschen99@nankai.edu.cn (Y. Chen).

¹ These authors contributed equally to this work.

shield, etc. Normally, it is described as the following equation:

$$SE = 10 \log \left(\frac{P_i}{P_o} \right) \quad (1)$$

In equation (1), P_i is the power of the incident wave, and P_o is the power of the transmitted wave. The transmission line theory proposed by Schelkunoff is the mostly used theory to explain the EMI shielding mechanism [9,10]. As shown in Fig. 1, when an EM wave is incident on the surface of the shield, there could be four different states for the EM wave. Firstly, due to the discontinuity of the wave impedance between free space and the shield, the surface of the shield will generate a great deal of reflection, which results in the reflection loss of EMI shielding. Secondly, some EM waves are not reflected by the surface of the shield, but enter the body and are then absorbed by the shield during the transmission. The energy could be converted into microcurrent or heat, which is called absorption loss. Thirdly, when the incident EM wave meets another surface of the shield or a heterogeneous interface inside the shield, it will also generate multiple internal reflections and scatterings, and this part of the attenuated energy is called multiple reflection/scattering loss. Lastly, some EM waves could still transmit through the EMI shielding materials, and spread further in its direction. Therefore, the total energy loss of electromagnetic wave can be regarded as the sum of three parts: reflection loss, absorption loss and multiple reflection/scattering loss [11,12]. According to the transmission line theory, EMI SE can also be expressed as equation (2):

$$SE = SE_R + SE_A + SE_M \quad (2)$$

Where SE_R is the single reflection loss on the material surface, SE_A is the absorption loss of the material, SE_M is the multiple reflection/scattering loss inside the material.

Recently, with the development of lightweight electronic communication equipment, the demand for EMI shielding materials has continued to increase worldwide [13–15]. It is estimated that the global EMI shielding material market will reach \$9.25 billion in 2025, with an increase of \$2.4 billion over 2020 [16]. Owing to this, various EMI shielding materials, such as metal-based materials, conductive polymer-based materials, carbon-based materials, and magnetic materials have been fabricated to satisfy the practical application [17–28]. These materials normally have high electrical conductivity or permeability, along with advantages such as cheap and accessible. However, they also suffer from problems like high density, poor mechanical property, and durability. Most importantly, those traditional EMI shielding materials mainly rely on reflection for the shielding of EM waves, rather than absorption of the incident waves, which would result

in non-negligible secondary pollution in actual applications [29–32]. In contrast, absorption-dominated EMI shielding materials can powerfully enhance the shielding effectiveness via initiative consumption, and can effectively avoid secondary pollution. Therefore, absorption-dominated EMI shielding materials are the focus of future research.

Different from traditional reflection-dominated EMI shielding materials, absorption-dominated EMI shielding materials avoid EM wave pollution made by the reflecting and scattering of the incident waves. Absorption-dominated EMI shielding materials usually owns high absorption coefficient (A), which is larger than the reflectivity coefficient (R). Therefore, the secondary pollution of EM waves could be largely reduced. In additions, those absorption-dominated EMI shielding materials could be also regarded as EM wave absorption materials, which has been widely used in military stealth fields.

Graphene aerogel is a newly-developing absorption-dominated EMI shielding material, which has ignited researchers' great interest since 2014 [12,33–40]. Graphene aerogels can be regarded as three-dimensional (3D) graphene assemblies made of graphene sheets or graphene-derivatives. Compared with traditional EMI shielding materials, graphene aerogels possess abundant advantages, such as an ultra-low density, a wide bandwidth from gigahertz (GHz) band to terahertz (THz) band, and a high compressibility helpful for various complex applications [34,41–46]. The excellent absorption-dominated EMI shielding performance is commonly attributed to the following three aspects. Firstly, graphene aerogel has high porosity up to 99%, and most EM waves prefer to incident inside the aerogel with low reflection. Secondly, the long-range interconnection network made of graphene sheets has mild electrical conductivity. The incident EM waves will induce microcurrent resulting in its attenuation, and finally converted into heat energy. Thirdly, the stacking and folding of graphene sheets inside the aerogel can significantly increase the reflection area for incident waves, extending the propagation path of incident waves, and finally enhance the multiple reflection/scattering loss and enhance the absorption-dominated shielding process. Owing to its superior performance, the reports of graphene aerogels as EMI shielding materials are increasing year by year, and the published articles related to graphene aerogels as EMI shielding materials have surpassed 600, as shown in Fig. 2a. In additions, the increasing granted Chinese invention patents also reflect its strong application value (Fig. 2b).

This review introduces the recent advances of graphene aerogels as absorption-dominated EMI shielding materials. Firstly, the fabrication strategies for graphene aerogel are summarized, and their advantages and disadvantages are both narrated. Then, EMI shielding materials based on graphene aerogels and their composites are classified, with their overall structure-performance relationship and absorption-dominated EMI shielding mechanisms discussed. Thirdly, smart and multifunctional graphene aerogel-based EMI shielding materials are highlighted as the future trend for EM functional applications. Lastly, the challenges and perspectives for graphene aerogels-based EMI shielding materials are summarized.

2. Fabrication of 3D graphene aerogels

Nowadays, graphene sheets have been assembled into various bulk materials, including one-dimensional graphene fibers [47,48], two-dimensional graphene films [49,50], and three-dimensional graphene aerogels [51,52]. Compared with graphene fibers and graphene films, the key for the fabrication of graphene aerogels is to construct a porous yet continuous network structure. Up to now, several methods have been developed for the fabrication of graphene aerogels. They could be easily divided into the following three categories, *i.e.*, assembly through physical/chemical interactions, assembly through templates, and chemical foaming method. These graphene aerogels prepared by different methods have different micro/nano structures, which also bring about different advantages and disadvantages to their properties.

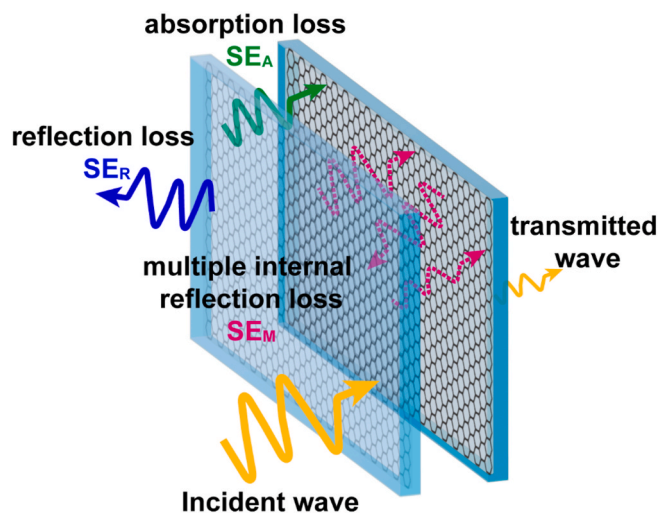


Fig. 1. Schematic diagram of EMI shielding mechanism.

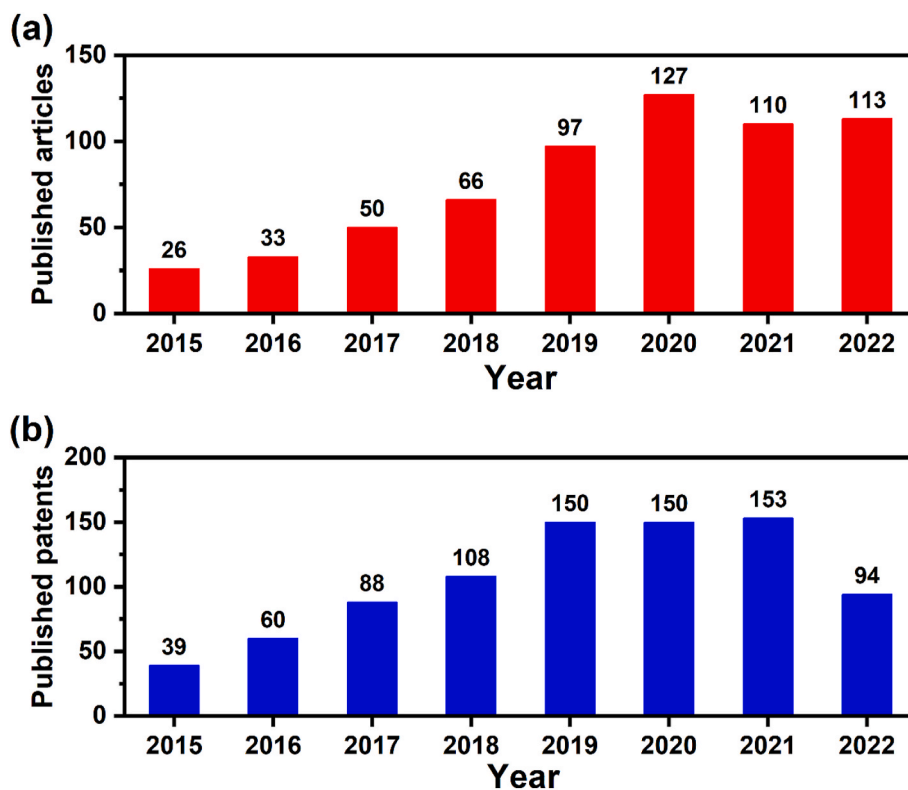


Fig. 2. (a) Number of articles published related to graphene aerogels as EMI shielding materials in the past few years; (b) number of granted Chinese invention patents related to graphene as EMI shielding materials in the past few years.

2.1. Assembly through physical/chemical interactions

2.1.1. Chemical crosslinking induced self-assembly

As is known, graphene derivatives, such as graphene oxides (GO), are usually decorated with plenty of functional groups, which can be used as the active sites for the chemical crosslinking of graphene sheets to construct 3D porous network. The generated chemical bonds between graphene sheets are relatively strong, making the network structure more stable with higher mechanical properties than those fabricated by other methods. Huang et al. reported a novel method to fabricate crosslinked graphene aerogels with edge-to-edge assembly [53]. La^{3+} or polyethylene imine were used as the crosslinking agents for the reaction with GO sheets. Owing to the special edge-to-edge crosslinking strategy, the obtained aerogels possess ultrahigh surface area (up to 850 m^2) and excellent mechanical properties (20 MPa for Young's modulus and 1 MPa for yield strength), make the resulting graphene aerogel a promising candidate in the field of environmental or mechanical engineering. Yao et al. prepared cellulose/reduced graphene oxide (RGO) composite aerogels via cation-induced gelation, during which celluloses and GO sheets were crosslinked by metal salt solution, followed by freeze-drying and chemical reduction to obtain the hybrid aerogels (Fig. 3a) [54]. Scanning electron microscope (SEM) images (Fig. 3b–d) show the randomly oriented interconnected 3D structures of hybrid aerogels, which exhibited excellent recoverability, superior absorption capacity for both organic solvents and water, and electrical conductivity sensitive to compressive strain.

2.1.2. Solvothermal reaction induced self-assembly

Besides the crosslinking by chemical reagents, solvothermal reaction is another commonly used method for the preparation of 3D graphene aerogels. Typically, GO solutions are placed inside a closed environment. As temperature increases, esterification reaction could spontaneously occur between the terminal groups of GO sheets (COOH, OH, and epoxy groups), and those GO sheets could be randomly crosslinked.

Additionally, the high temperature environment also facilitates the reduction of GO sheets, endowing aerogels with higher electrical conductivity.

Hydrothermal process of graphene aerogel in a $180 \text{ }^\circ\text{C}$ Teflon-lined autoclave has been widely used by researchers since 2012 [55]. Wan et al. found that the hydrothermal reaction time strongly affects the final morphology of graphene aerogel [56]. A short time (4h) is unable to form a firm interaction between graphene sheets. With extending time of 12h, a tightly connected graphene skeleton could be generated, and the corresponding mechanical performance and electrical conductivity will be also improved. Owing to the convenience of solvothermal reaction, various graphene-based composite aerogels have been fabricated, including graphene/polymer aerogels, graphene/metal oxide aerogels, and graphene/MXene aerogels. For example, Yin et al. has prepared novel iron nitride/graphene aerogel by a facile two-step hydrothermal process [57]. As shown in Fig. 4, iron phthalocyanine (FePc) nanoparticles were firstly adhering to GO sheet, then they went through the hydrothermal process. As a result, iron phthalocyanine is uniformly dispersed and anchored on graphene surface with the assist of π - π stacking, and finally endows it with excellent oxygen reduction reaction performance. Besides, a series of heteroatom-doping graphene aerogels (N-doped, S-doped aerogel et al.) were prepared in those hydrothermal reactions, by introducing co-reaction reagents and further thermal annealing treatment [58–60]. These composite aerogels have demonstrated great performance in various fields, such as strain sensing, energy storage and conversion, electromagnetic wave shielding and absorption, and electrochemical catalysis [61–64].

2.1.3. Chemical reduction induced self-assembly

Although hydrothermal reaction can bring about ordered three-dimensional graphene skeletons, the high temperature and long reaction time limit its practical applications. For comparison, chemical reduction of GO solution is commonly implemented under a relatively low temperature environment (60 – $100 \text{ }^\circ\text{C}$), and the three-dimensional

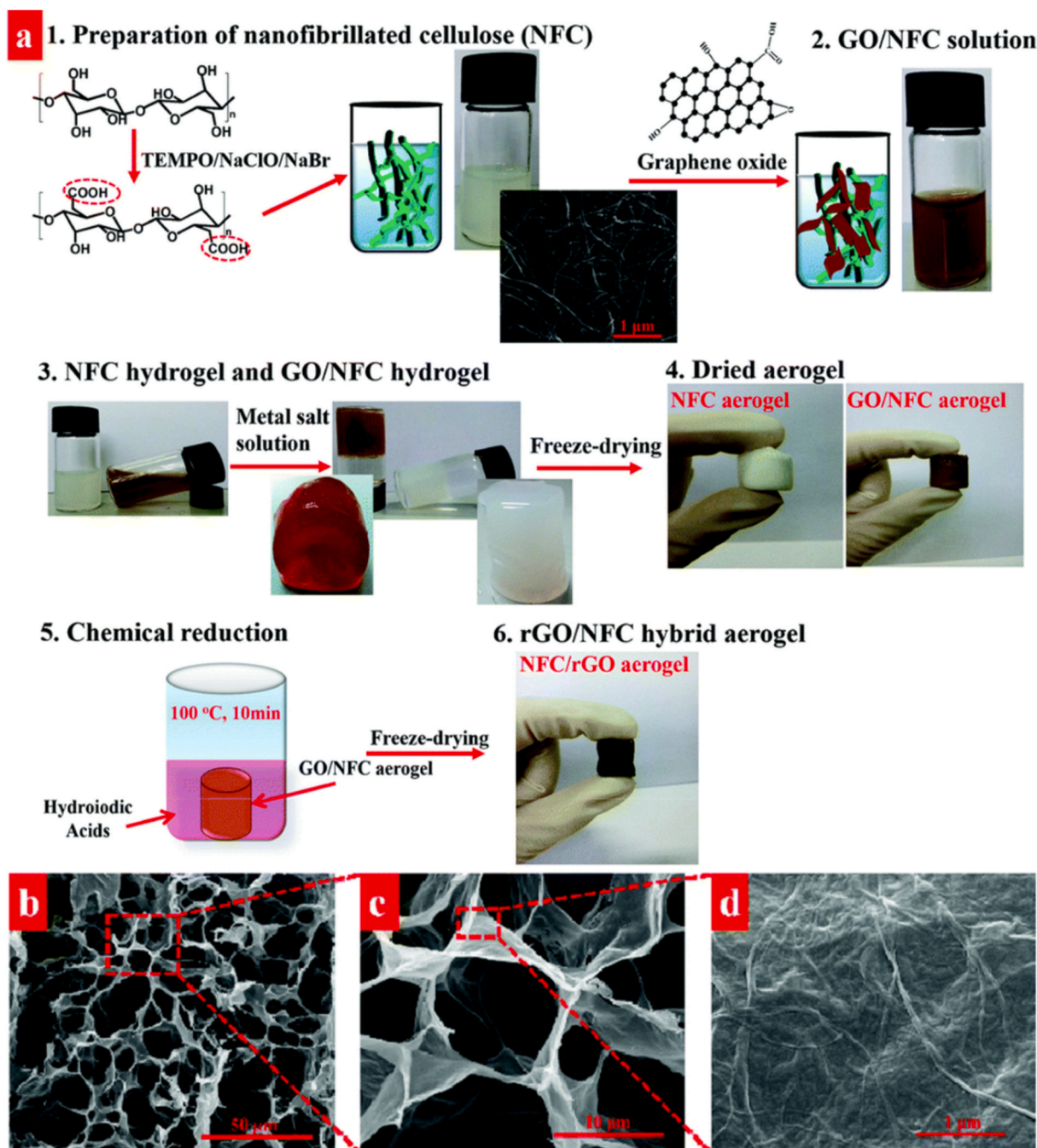


Fig. 3. (a) Fabrication process of cellulose/RGO aerogel via cation-induced crosslinking; (b, c, d) SEM images of composite aerogels with different magnifications. Reprinted with permission from Ref. [54].

network could be also constructed via the reduction-induced π - π interactions. Chemical reagents, such as ammonia, hydrogen iodide (HI), hydrazine hydrate (N_2H_4), ethylenediamine (EDA), and Vitamin C, are widely used as reducers. Under a mild environment, the GO solutions could get slowly reduced, and many O-containing groups are eliminated, resulting in the formation of RGO sheets. Thus, the π - π interactions between RGO sheets would be greatly enhanced, and the adjacent sheets started to aggregate, finally leading to the fabrication of 3D graphene hydrogels. Commonly, the reducing degree could be regarded as the most important parameter during the reaction, and it is usually affected by the reaction time, the content of reducing agent, and the temperature. Compared with hydrothermal reaction, the fast preparation process enlightened the method with more potential applications in the future.

For example, Li et al. prepared the 3D graphene hydrogel by the reduction of Vitamin C for only 1 h, much lower than that of hydrothermal reaction (8–15 h) [65]. Besides, various kinds of reducing agents have been studied for the synthesis of graphene hydrogels by Chen et al. [66]. It is found that the required time for hydrogel formation is different. It takes 30 min for NaHSO_3 while it requires only 10 min for Vitamin C and Na_2S . In additions, some composite aerogels have been prepared using this method, such as polymer/graphene aerogel, metal/graphene aerogel. For example, Wang et al. fabricates the RGO/Al/ Bi_2O_3 composite aerogels by chemical reduction and gelling (Fig. 5), using EDA as reducers [67]. The initial gelling process only takes 10 min, and it was then freeze-dried to remove solvent, and porous composite material was finally obtained.

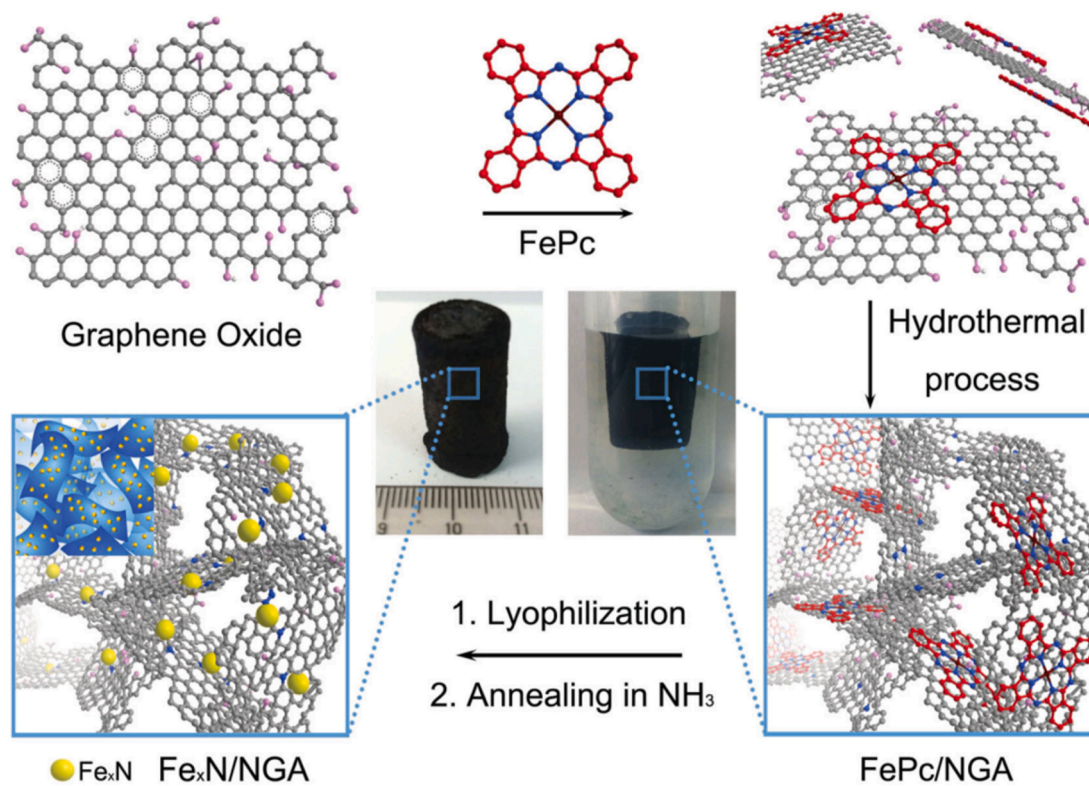


Fig. 4. Hydrothermal procedure for the preparation of FeN/graphene aerogel. Reprinted with permission from Ref. [57].

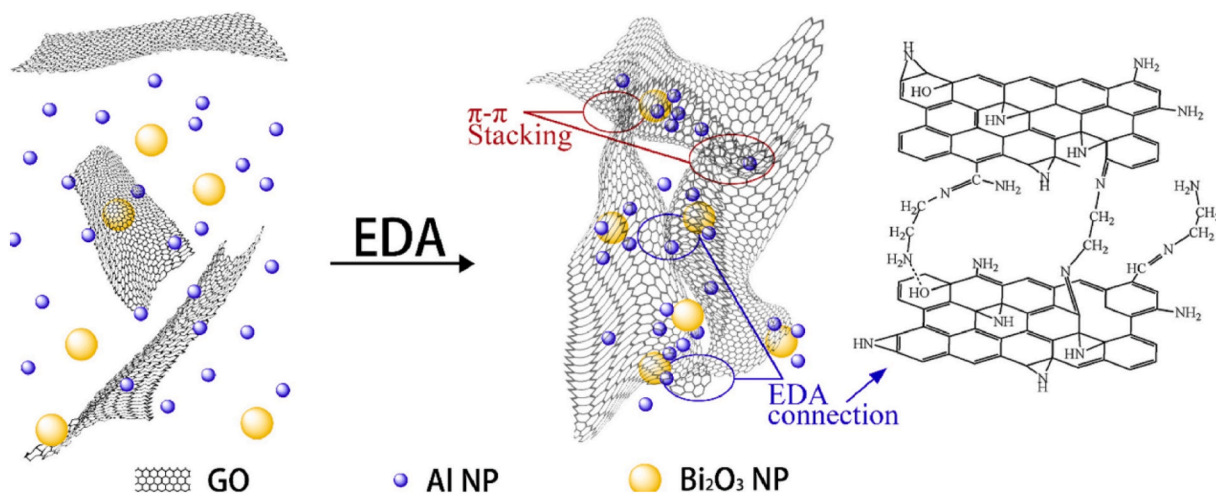


Fig. 5. Formation mechanism of RGO/Al/ Bi_2O_3 gel. Reprinted with permission from Ref. [67].

2.2. Assembly through templates

2.2.1. Ice template method

Ice template is the most popular method for the preparation of graphene aerogels. Any laboratory equipped with a freeze-drying device (such as refrigerator and freeze dryer) can fabricate the aerogels, so that the preparation process is easy and cost-effective. Commonly, those GO solutions are placed in a freezing equipment, such as liquid nitrogen-freezing device or refrigerator. The water slowly turns into ice, with GO sheets expelled into the ice crystal edge, or between ice crystals. Further, the frozen GO solution goes through the freezing-drying process, and the graphene aerogel is fabricated. A noteworthy advantage of the ice-template method is its designability, and the micro/nano architecture of aerogel could be effectively tailored during the ice-formation

process. Specifically, the final architectures of graphene aerogel such as its porosity, and orientation, can be tuned by the designing of ice nucleation and growth process. The most famous example is the aligned graphene aerogel. For example, Yang et al. fabricate a biomimetic long-range ordered 3D graphene structure by using a polydimethylsiloxane (PDMS) wedge with a slope angle of around 15° , generating temperature gradient in both horizontal and vertical direction [68]. Liu et al. demonstrated a calcium ion-assisted unidirectional-freezing approach for fabricating highly anisotropic graphene aerogels by unidirectionally freezing aqueous suspensions of GO with a trace amount of calcium ions (Fig. 6a), followed by freeze-drying and thermal reduction [69]. The aerogel exhibits a highly oriented and regulated architecture, in which the graphene sheet walls are nearly parallel to its transverse direction (Fig. 6b–e). Yang et al. simulated the microstructure of graphene aerogel

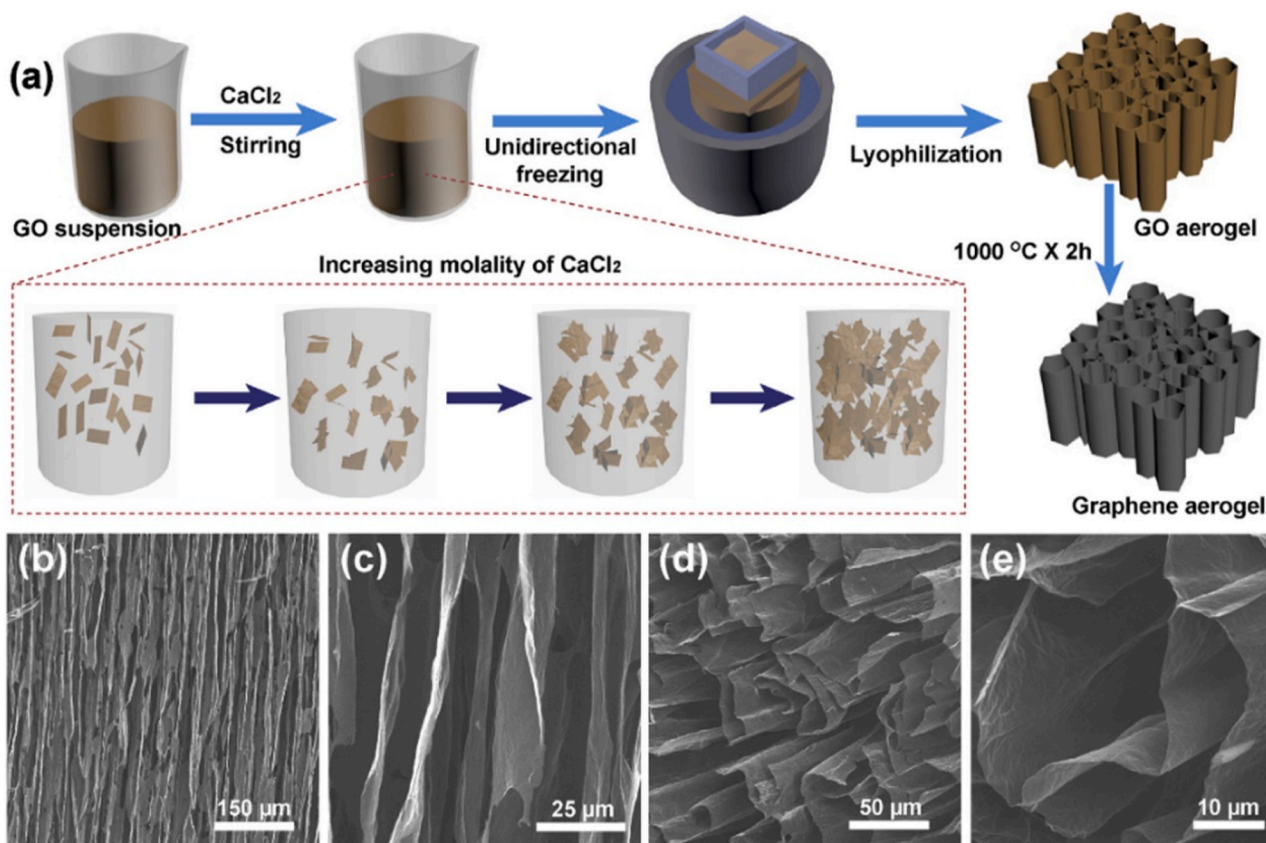


Fig. 6. (a) Schematic illustrating the fabrication of anisotropic graphene aerogel; high-magnification SEM images of GO5-2.5 along (b, c) transversal and (d, e) longitudinal direction. Reprinted with permission from Ref. [69].

formation during the water freezing process [70]. The results show that the morphology and size of graphene wall structure in aerogel are derived from the comprehensive effects of ice nucleation, polycrystalline growth and graphene diffusion. Nevertheless, due to the relatively insufficient direct contacts of graphene sheets, the chemical/physical interactions between individual graphene sheets are weak for ice-template aerogels, which results in much lower mechanical performance and electrical conductivity, compared with that of the chemical crosslinking/reduction strategies.

2.2.2. CVD method

Chemical vapor deposition (CVD) is another widely used method for the preparation of graphene aerogels. Commonly, CVD involves a one-step synthesis based on the breaking of precursor molecules (gas, liquid, and solid) in the gaseous state and their reforming over a substrate/catalyst. For the fabrication of graphene aerogels/foams, the carbon atoms are directed deposited on the templates, such as metallic frameworks (Ni/Cu foam), oxides (MgO powders), biomorphic templates (seashells), minerals (zeolites), as well as dielectric substrates (Al_2O_3), with the aid of catalysts in high temperature environment. Compared with the chemical/physical interaction assembling method, the fabricated graphene aerogel by CVD method possesses high crystallinity and lower defects. Cao et al. prepared a novel 3D graphene network using Ni foam as a sacrificial template in a facile CVD process, with ethanol as the carbon source [71]. The whole CVD process is carried out in a 1000 °C chamber for only 10 min. The production can be easily scaled up by using a larger CVD chamber, which is more essential for practical applications. Xu et al. further employed a combination of conventional CVD with additive manufacturing for graphene aerogel growing [72]. A sacrificial silica template with complex-designed structures prepared by 3D-printing techniques enables the fabrication

of crack-free graphene foam. Such synthesis collaboration enables a hierarchically constructed 3D graphene foam with a large surface area, excellent conductivity, and good mechanical properties (Fig. 7). Besides the pure graphene aerogel, many doped 3D graphene structures have been reported through the CVD method, and various foreign atoms (such as N, B, S, and P) have been incorporated into 3D graphene framework by the high temperature treatment procedures [73–76].

2.3. Chemical foaming method

Direct foaming from solids is the most efficient method to fabricate porous materials, and this is widely applied for the fabrication of polymer foam. However, the direct foaming of pure nano-materials is commonly impossible, because the plasticity of their solids is denied by the overwhelming interface interactions. Recently, Gao's group has successfully invented a chemical foaming method to directly convert GO solids into aerogel bulks [77–80]. The GO films were firstly prepared by cast-drying. Then, the GO films were immersed into the $\text{N}_2\text{H}_4/\text{H}_2\text{O}$ solution for water intercalation and plasticization (Fig. 8a). Water molecules penetrated the GO interlayer gallery and the intercalation was completed in a few seconds. The interlayer spacing increased from 0.90 nm in dried GO to 2.32 nm in plastic GO solid, which was confirmed by X-ray diffraction spectra. In the following chemical foaming process, the reaction of N_2H_4 with oxygen-containing groups of GO sheets exhausted gas (such as CO_2 and H_2O) and produced bubbles in the interlayer space, thus generating pores inside graphene sheets (Fig. 8b/c). In the final drying process, water was directly evaporated by heating to avoid unnecessary freeze drying and solvent replacement process, and the hydroplastic graphene aerogel (HGA) was fabricated. The morphology of graphene aerogel fabricated by chemical foaming is very different from that of direct freezing. The face-to-face configuration of graphene

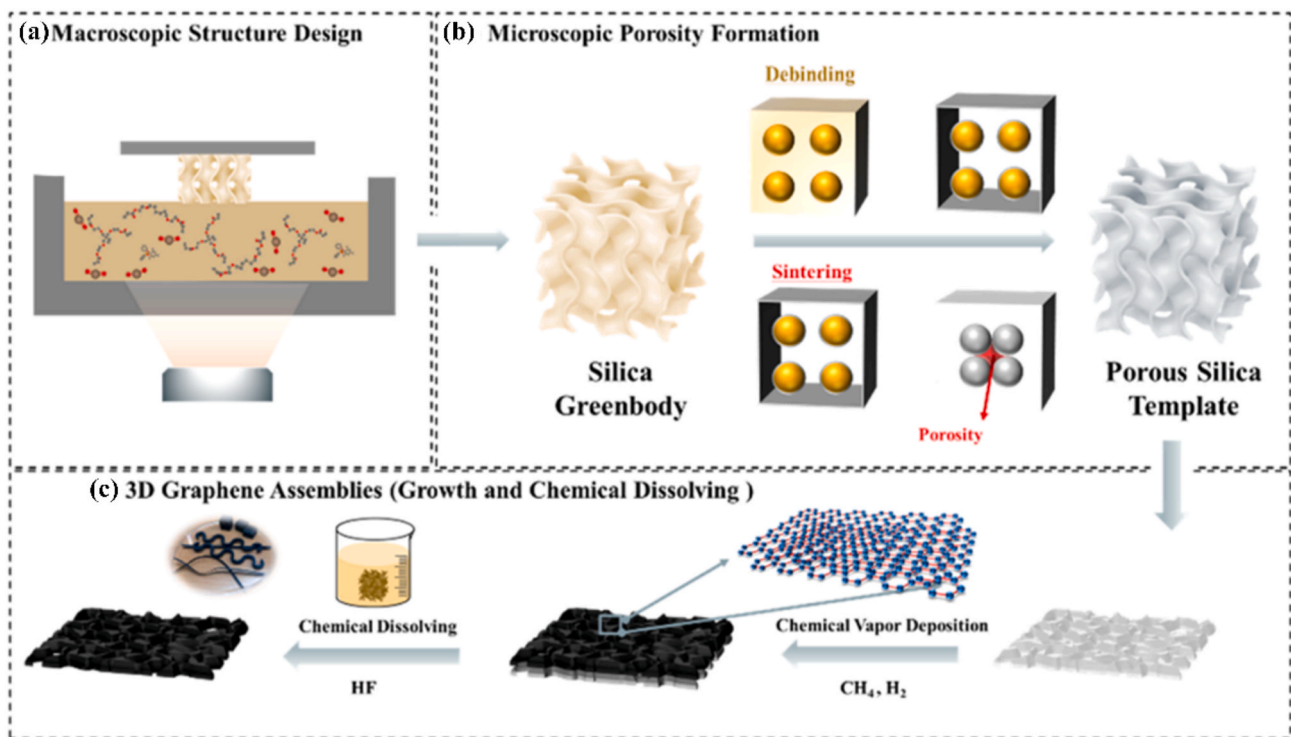


Fig. 7. Preparation methods involved in fabricating 3D graphene assembly. (a) 3D printing of silica green body (macroscopic structure design); (b) debinding of polymer additives (or ligand removal) and sintering procedure for porosity formation; (c) CVD and wet etching of a sacrificial silica template to form 3D graphene assemblies. Reprinted with permission from Ref. [72].

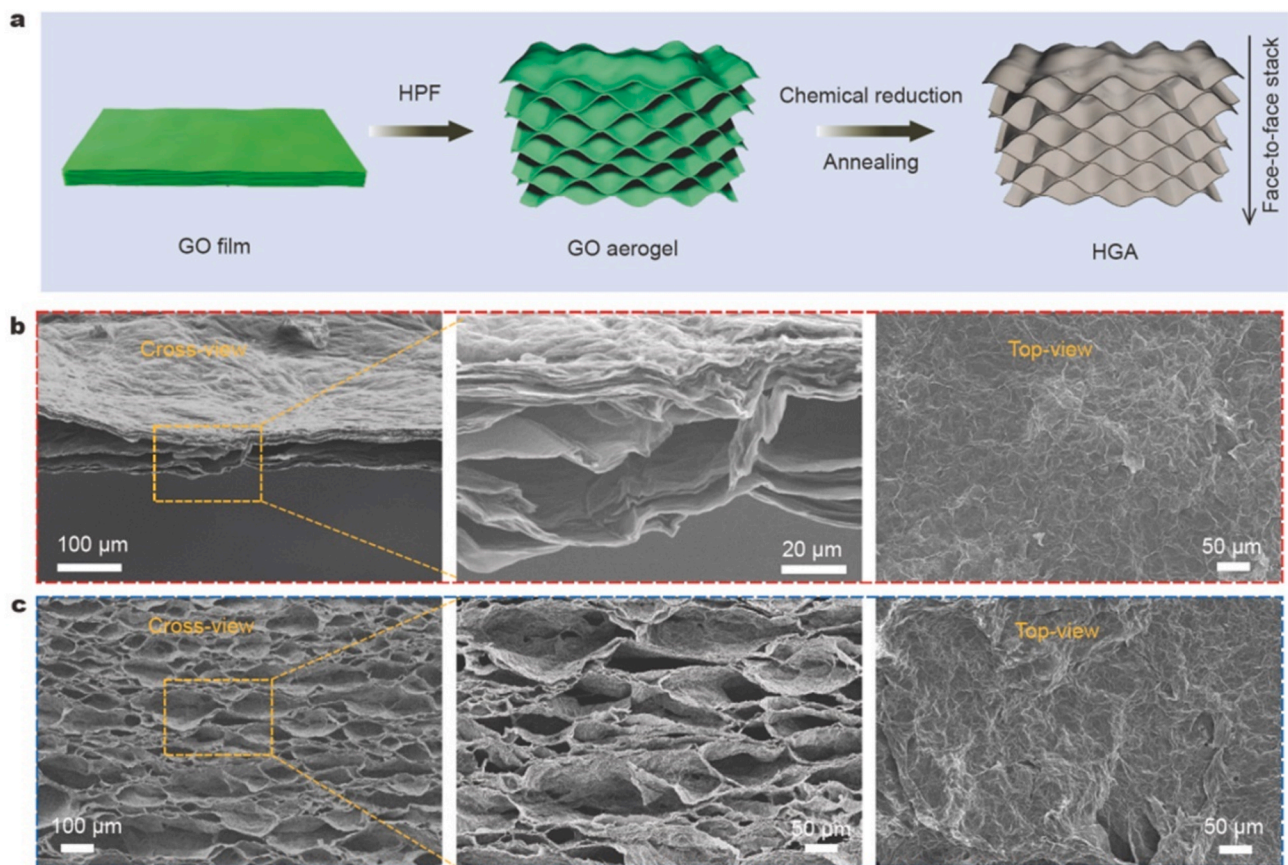


Fig. 8. (a) Schematic illustration of the fabrication processes of HGA; cross-section view and top-view SEM images of GO film (b) and HGA (c). Reprinted with permission from Ref. [80].

walls dominates to form a hyperboloid structure by bubble clustering, instead of random configurations in freezing-dried aerogels, and this renders graphene aerogels with ultra-robust mechanical stability against extreme deformations.

3. Graphene-based aerogels for EMI shielding

3.1. Pure graphene aerogel for EMI shielding

Graphene aerogels are widely used as electromagnetic protection materials since 2014. Chen et al. firstly reported the fabrication of

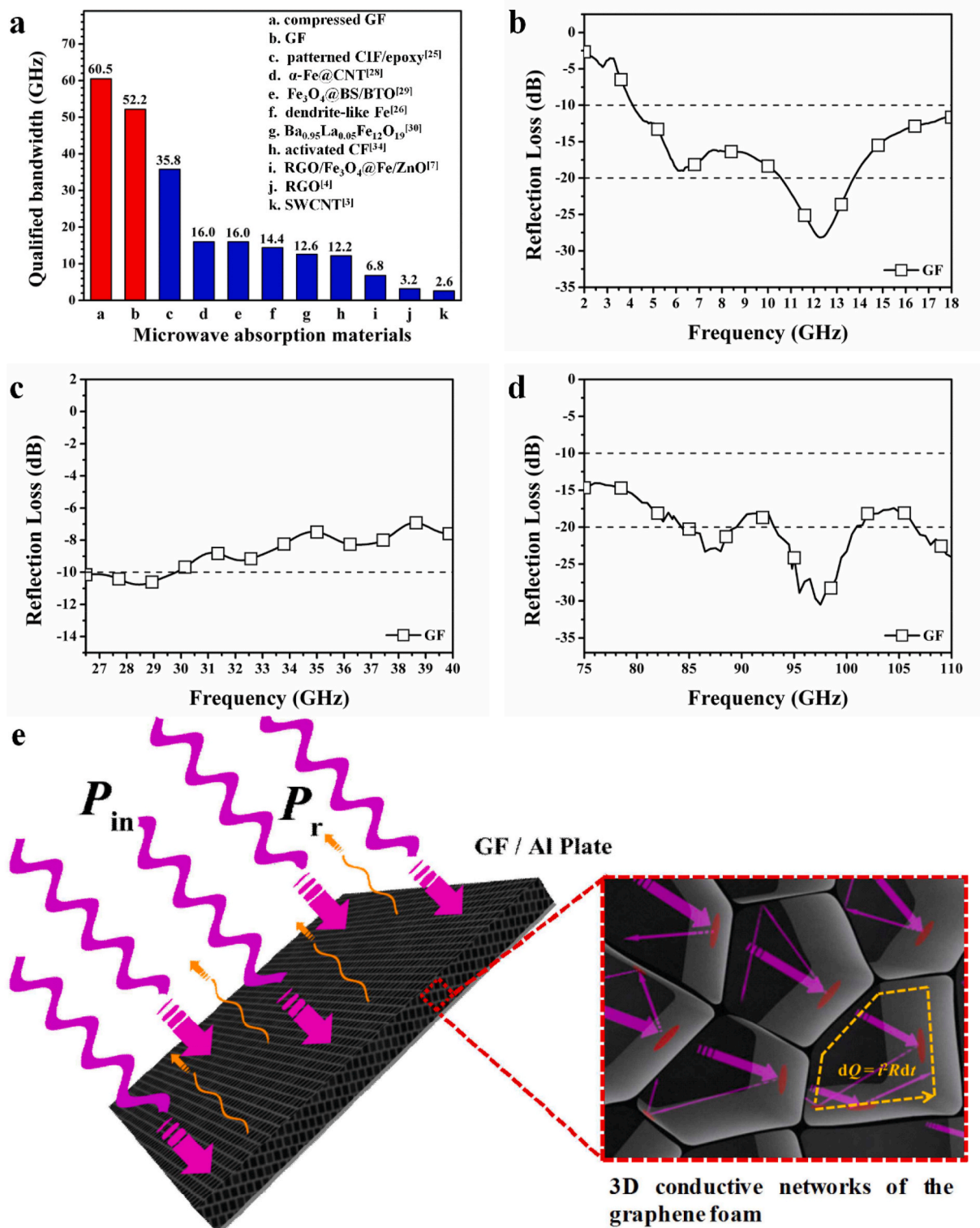


Fig. 9. (a) Direct comparison of the MA performance of the solvothermal-fabricated graphene aerogels with those of the representative material; the RL curves for the pristine graphene aerogels are shown in (b) 2–18 GHz; (c) 26.5–40 GHz; and (d) 75–110 GHz; (e) schematic representation of the MA mechanism for the graphene aerogel. Reprinted with permission from Refs. [82].

graphene/PDMS foam as strong EMI shielding materials [81]. In their experiments, Graphene with high quality was grown on a Ni foam by CVD method. Then, a thin layer of PDMS was coated on the surface of graphene, followed by the etching of Ni foam. The lightweight foam with a density of 0.06 g/cm^3 owns a shielding efficiency of 30 dB in the 30 MHz–1.5 GHz band and 20 dB in the X band. As can be seen, the graphene foams fabricated by the CVD method display strong EMI shielding performance. However, such a CVD-fabricated low-defect graphene foam possesses “perfect” lattice structure, which endows it with high conductivity, and the high shielding efficiency is mostly attributed to the reflection of microwaves, rather than absorption. In contrast, Zhang et al. fabricated a RGO foam via the solvothermal method with the effective microwave absorption performance [82]. The effective absorption bandwidth (EAB, definition of the bandwidth where

reflection loss (RL) is under -10 dB) of 50.5 GHz, was vastly superior to many reports. Moreover, via 90% physical compress strain, the EAB of aerogel experienced an increase to 60.5 GHz, showing the potential of graphene aerogel for adjustable electromagnetic protection applications (Fig. 9a–d). In 2018, Huang et al. further discovered the high absorption efficiency of RGO aerogel to THz waves [83]. An ultra-wide EAB that covers 95% of the entire measured bandwidth from 0.1 to 1.2 THz was achieved, which demonstrated that graphene aerogel is a multi-band compatible EM wave absorbing material, suitable for both GHz and THz waves. Compared with CVD-fabricated graphene foam, the solvothermal reaction of GO solution could only partially eliminate the defects of GO sheets, and the electrical conductivity of obtained network was only in the range of 10^{-1} – 10^{-5} S/m , far lower than that of CVD-fabricated one. Combined with its porous structure, the delicate

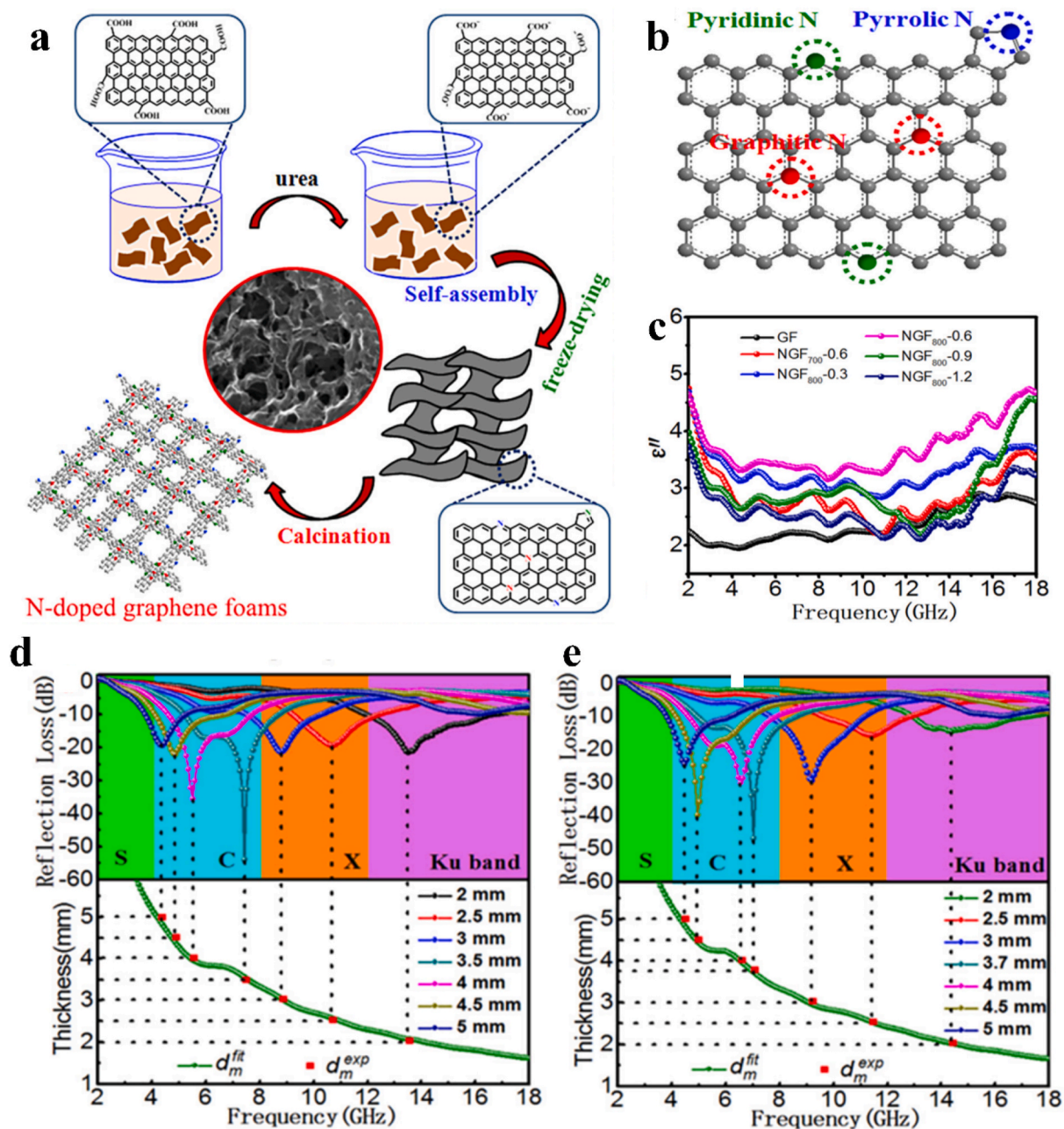


Fig. 10. (a) Schematic illustration for the formation of N-doped graphene foams via the induction of urea in the hydrothermal reaction; (b) three kinds of N bonding configurations; (c) imaginary part of N-doped graphene foams; (d, e) frequency dependence of RL curves and the matching thickness versus peak frequency of three N-doped graphene foams. Reprinted with permission from Ref. [88].

construction of the 3D network brought about excellent impedance matching between the RGO aerogel and air, and the EM wave could easily incident inside the aerogel, rather than been reflected. Then, the long-range mild conductive network consisting of entangled conductive

graphene sheets could intensely respond to the broadband incident microwave as tremendous resistance–inductance–capacitance coupled circuits, which could effectively dissipate the microwave energy. Besides, the incident microwave could be further scattered and reflected

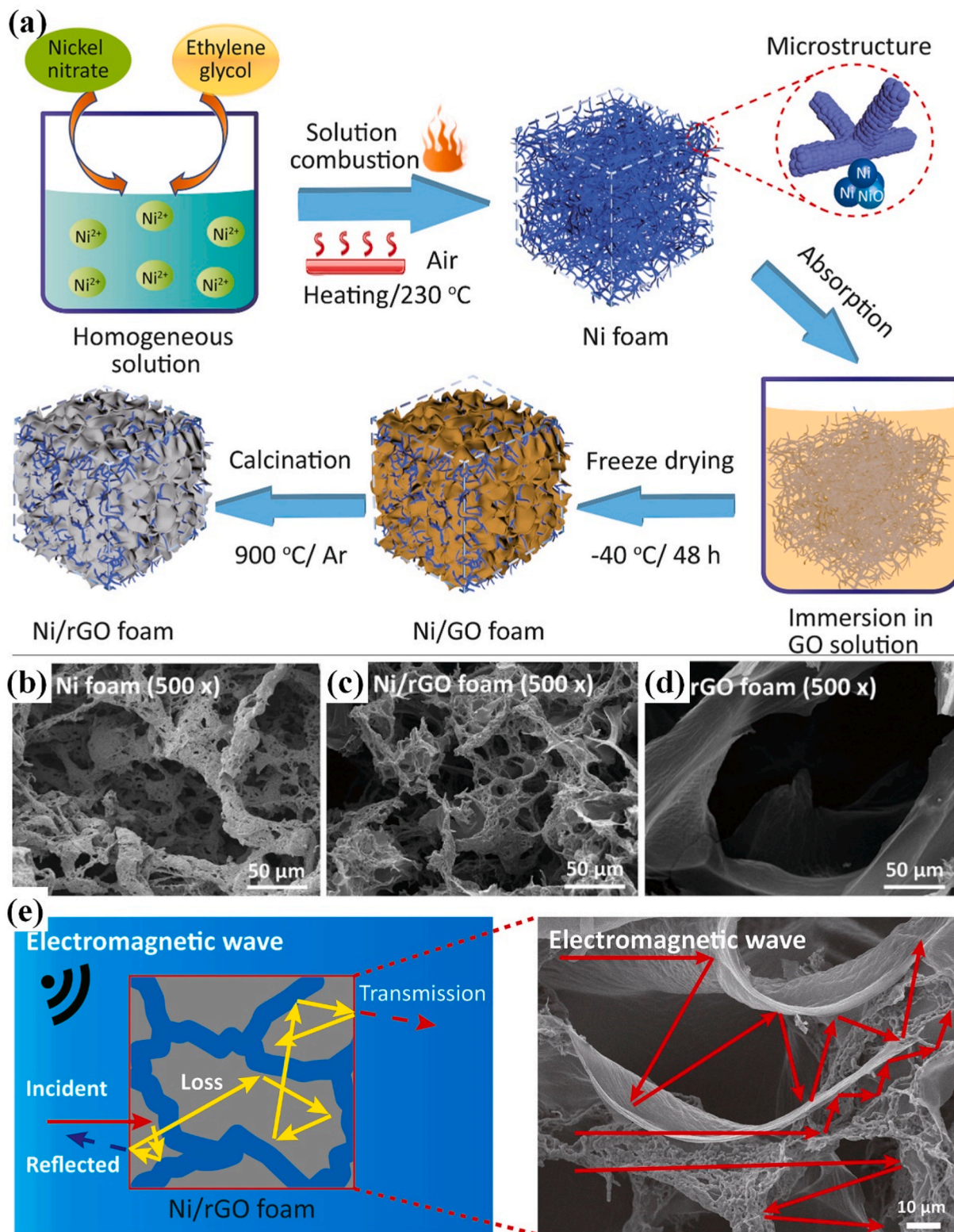


Fig. 11. (a) Schematic illustration of the fabrication process of the Ni/RGO composite foam; microstructural images of (b) Ni foam, (c) Ni/RGO foam, and (d) RGO foam; (e) schematic diagrams of possible EM wave attenuation mechanism in Ni/RGO foam. Reprinted with permission from Ref. [89].

inside the porous structure (Fig. 9e), when it encounters the pore wall made of graphene sheets, and this finally promoted the absorption of EM waves.

3.2. Heteroatom doped graphene aerogel for EMI shielding

Doping heteroatoms for carbon materials has attracted extensive attention in recent years. Nitrogen atoms are considered excellent candidates for chemical doping of carbon materials, because of their comparable atomic size and their 5 valence electrons which can form strong covalent bonds with carbon atom. Furthermore, N-doping can reduce the intrinsic resistance of graphene, which facilitates the transfer of electrons through the active material. Liu's group has long been investigating doped carbon materials as microwave absorbers/shields [84–86]. In 2018, Zhou et al. prepared N-doped graphene (NG) composite aerogels as EM wave absorption materials [87]. The authors claimed that N atoms can break the sp^2 domains of graphene hexagonal lattice, thereby forming disordered sites, resulting in defect polarization relaxation and electron dipole polarization relaxation, both of which are beneficial to improve the dielectric loss for microwaves. The NG composite aerogel has good EM absorption performance in the Ku-band, with the minimum value of RL of -53.25 dB and the EAB value of 8.15 GHz. In 2019, Liu et al. reported N-doped graphene foams with high porosity and open reticular structures [88], which were also prepared via self-assembled hydrothermal reaction, freeze-drying, and 800 °C treatment (Fig. 10a). The X-ray Photoelectron spectroscopy results demonstrated that three different kinds of N bonding configurations, pyrrolic/pyridinic/graphitic, all exist inside the graphene skeleton (Fig. 10b). Since N atoms can act as electron donors and donate free electrons to the conjugated system properties, it induces a great improvement in their electrical conductivity. The investigation of N bonding configurations illustrates that the presence of pyrrolic/pyridinic N is essential for the dipolar relaxation loss whereas graphitic N is beneficial to the conduction loss (Fig. 10c) for microwave dissipation, thus leading to strong EM wave absorption capacity and broad absorption bandwidth simultaneously (Fig. 10d–e).

3.3. Graphene-based composite aerogel for EMI shielding

3.3.1. Metal/graphene composite aerogel

Metals are natural excellent EMI shielding materials, which usually have high electrical conductivity. Several kinds of metals are used for the preparation of metal/graphene composite aerogels. Among all those metal materials, nickel has been conspicuous in the past few years, on account of its excellent conductivity and magnetic susceptibility. So, it is considered as the preferred option to composite with graphene aerogels, in order to compensate for monotonous dielectric loss of graphene for EMI shielding/microwave absorption. Numerous methods have been explored to integrate nickel and graphene as aerogel materials. Liu et al. fabricated an ultra-light nickel/graphene composite foam by a combination of solution combustion, freeze-drying, and high temperature annealing (Fig. 11a) [89]. The resulting Ni/RGO foam displayed an interpenetrating network consisting of the 3D Ni skeleton and continuous RGO sheets, as shown in Fig. 11b/c/d. The 3D interpenetrating conductive network enriched and refined the pore size for Ni foam, also created numerous Ni/graphene interfaces, and thus assisted to achieve eminent impedance matching for broadband microwave absorption and EMI shielding. Due to multiple loss mechanisms created by the interpenetrating network of Ni and RGO sheets, the Ni/RGO composite foam projected a high absorption-dominated shielding efficiency (Fig. 11e). It achieved a minimum RL of -53.11 dB at 6.08 GHz and an EAB of 4.91 GHz for EM absorption.

Gao et al. prepared a Ni-chains/RGO microcellular foam with an asymmetrical conductive structure [90]. An RGO-rich layer and a Ni-chains-rich layer were placed on both sides of the aerogel via hot pressing and supercritical carbon dioxide foaming process. Benefiting

from the construction of an asymmetrical conductive structure, the microcellular foam with 5 vol% RGO and 5 vol% Ni-chains exhibits good electrical conductivity ($\sim 10^{-1}$ S/m) and high EMI SE value (40.82 dB) in X-band. Besides, the maximum difference of reflection coefficient (R) is up to 0.5 by actively regulating the EM wave incidence direction (Ni chain-rich side or RGO-rich side), demonstrating its tunable absorption/reflection performance for EM waves.

Besides Ni metals, some high conductive metal materials (Ag and Cu) are also investigated for the preparation of graphene composite aerogel as EMI shielding materials. Liang et al. prepared 3D silver plates/RGO foams (AgPs/rGF) with numerous regular spherical hollow structures [91]. Ag plates achieved uniform dispersion along the 3D RGO network via a sol-gel template method. The composite showed a maximum EMI SE value of 58 dB and an electrical conductivity of 45.3 S/m, demonstrating huge enhancement made by two-dimensional metal nanoparticles. Gao et al. combined one-dimensional Ag nanowire (NW) and 3D graphene foam to prepare a 3D AgNW/graphene bicontinuous conductive skeleton through a hydrothermal reduction method and thermal annealing process [92]. The AgNWs are uniformly dispersed on the surface of graphene sheets, with a high aspect ratio. Besides, the AgNW interconnected with each other tightly, generating a bicontinuous conductive network along with the graphene foam. The electrical conductivity increased from 26.5 S/m to 498 S/m when the mass ratio of AgNW to GO increased from 0 to 50, demonstrating the essential effect of AgNW. Benefiting from the construction of the efficient bicontinuous conductive network, the composite aerogels achieved the highest EMI SE value of 84.01 in the X band, which shows the great application value as high-performance EMI shielding materials. Yang et al. synthesized copper nanowires/thermally annealed graphene aerogel with high electrical conductivity [93]. The composite has shown dual functions of thermal conductivity and EMI shielding, with an EMI SE of 47 dB and electrical conductivity of 120.8 S/m, which is ascribed to perfect 3D Cu nanowires-graphene conductive network structures.

3.3.2. Magnetic material/graphene aerogel

Although metal/graphene composite aerogel exhibited excellent electricity conductivity and high EMI SE value, most of them provide a reflection-dominated shielding mechanism and weakened impedance mismatch, which is obviously not the optimal composite material for EMI shielding. Therefore, magnetic materials have caught researchers' eyes to enhance the impedance matching for the composite aerogels. Besides, magnetic materials provide magnetic loss mechanism differing from the dielectric route of graphene aerogel, which would significantly enhance its absorption and shielding performance. Within all distinguished magnetic materials, ferromagnetic materials possess the capacity of strong magnetism, which makes them an ideal component for absorption-dominated graphene aerogel. Researchers have developed several novel methods to fabricate the graphene/ferrites composite aerogel. Fang et al. has prepared Fe_3O_4 /graphene composites aerogels [94]. The Fe_3O_4 spheres were in-situ grown on graphene foam networks via the assistance of polydopamine (PDA) layers. The signally hierarchical architecture gave rise to multiple interfaces between the nanoparticles and graphene sheets. The intricate porous architecture inside the Fe_3O_4 spheres formed a microcosmic district that coordinated with the porous structure of the macroscopic graphene aerogel, permitting the transferring/dissipation of multiple electromagnetic waves with different frequencies, according to the $1/4$ wavelength theory. In addition, natural resonance and exchange resonance were enhanced. As a result, the magnetic loss was increased and thus improved the overall EMI shielding values. The graphene/ Fe_3O_4 /PDMS composite aerogels have achieved a high average EMI SE value of 70.37 dB in the X band, which made a 22 dB enhancement compared with graphene aerogel without the loading of Fe_3O_4 .

Zhu et al. fabricated a Fe_3O_4 /graphene foam (GF) composite using a CVD method. Conductive graphene foam was firstly prepared by CVD [95], and cetyltrimethylammonium bromide (CTAB)-modified magnetic

Fe_3O_4 nanoparticles were assembled on the conductive graphene by mutual electrostatic attraction, then it was encapsulated by PDMS. The lightweight $\text{Fe}_3\text{O}_4/\text{GF}/\text{PDMS}$ composite reaches a high EMI SE of 32.4 dB in the X band, showing obvious advantage comparing with single GF/PDMS or $\text{Fe}_3\text{O}_4/\text{PDMS}$ composites. Huangfu et al. functionalized Fe_3O_4 with EDA, using a template-casting method to fabricate Fe_3O_4 -thermally annealed graphene aerogel nanocomposites [96]. The obtained composite presented an EMI SE of 35 dB in the X band. Luo et al. prepared a sandwich-like buckypaper/yttrium iron garnet (YIG)-graphene aerogel/buckypaper metacomposite [97]. The composite exhibited a double negative electromagnetic behavior and excellent EMI shielding performance due to the high magnetic permeability of YIG and the novel construction of the composite, and an EMI SE value of 70 dB was achieved with the thickness of 4 mm. Besides Fe_3O_4 , other magnetic oxides have also been adapted for compositing with graphene aerogels. Cobalt-zinc ferrite exhibits outstanding electromagnetic properties such as strong anisotropy, excellent mechanical hardness, high saturation magnetization and first-class chemical stability. Shu et al. fabricated cobalt-zinc ferrite/graphene composite aerogel with a minimum RL of -66.8 dB for EM absorption in the X band, with a thickness of 2.6 mm [98]. A broadband EAB of 5.0 GHz could be achieved at a thickness of only 1.6 mm. It is important that the magnetic cobalt-zinc ferrite endows the composite aerogel with ferromagnetic behaviors which brought about enhancement in magnetic loss routes, including natural resonance, exchange resonance, and eddy current loss. Wang et al. prepared unique $\text{CoFe}_2\text{O}_4/\text{N-RGO}$ aerogel by embedding CoFe_2O_4 nanoparticles into N-doped RGO via facile solvothermal methods [99]. The electromagnetic parameters of composite aerogels can be immensely improved by tuning the additive amount of CoFe_2O_4 nanoparticle. An optimal microwave absorption performance is achieved when the mass ratio of GO to CoFe_2O_4 is 1:2, with highest EAB up to 6.48 GHz (11.44–17.92 GHz) and best RL value of -60.4 dB.

3.3.3. MXene/graphene composite aerogel

In the past few years, two-dimensional transition-metal carbides (MXene) with versatile surface chemistry, high aspect ratios, and superior electrical properties have been intensively exploited for different kinds of potential applications, such as energy storage, catalysis, sensing, and EMI shielding [100–102]. The two-dimensional sheet-like structures of MXenes are ideal for compositing with graphene as aerogel materials for EMI shielding and microwave absorption, which has ignited researchers' interests.

In 2018, Zhao et al. developed a GO-assisted hydrothermal assembly method for the preparation of graphene/MXene composite aerogel (Fig. 12a) [103]. The resultant hybrid aerogels exhibit aligned cellular microstructure, in which the graphene sheets serve as the inner skeleton, while the compactly attached $\text{Ti}_3\text{C}_2\text{T}_x$ sheets present as shells of the cell walls. The composite foam exhibited great electrical properties, highlighting the crucial contribution of $\text{Ti}_3\text{C}_2\text{T}_x$ to the composite aerogel, and this further endow its epoxy nanocomposite with an outstanding EMI SE value of more than 50 dB in the X band at a low $\text{Ti}_3\text{C}_2\text{T}_x$ content of only 0.74 vol % (Fig. 12b). As is shown in Fig. 12c/d, the fracture surface of MXene/graphene aerogel (MGA) and its epoxy nanocomposite showed highly aligned cell walls, indicating the aligned $\text{Ti}_3\text{C}_2\text{T}_x$ network is well retained in the nanocomposite. The interconnected conductive network and the highly aligned architecture provided multiple and unobstructed paths for incident electromagnetic waves, thus resulting in the superior electrical and EMI shielding properties.

In 2019, Ma et al. investigated the THz absorption performance of MXene/GO composite foam fabricated by the solvothermal method [104]. The results demonstrated that the thickness and MXene content play a crucial role in its THz stealth performance. After the addition of MXene, the adsorption performance of composite foam is greatly improved compared to pure GO foam, with an optimal average THz RL value of 30.6 dB. In 2022, Jin et al. fabricated a multifunctional

MXene/graphene/polymer composite with a three-dimensional conductive network via a facile dispersion dip-coating approach [105]. After the dip-coating procedure, the MXene and graphene nanosheets can be uniformly deposited on the PU network, and the open micropores of the PU sponge are filled with MXene and graphene nanosheets. The composite aerogel exhibited a highest EMI SE of 43.3 dB in the X band with a thickness of 2.4 mm.

Although MXene facilitates the graphene aerogel with high conductivity, it also weakens the absorption performance of aerogel due to the impedance mismatch with air, and the dominated EMI shielding mechanism for most MXene/graphene aerogel is reflection rather than absorption. To solve the problem, many researchers have prepared graphene/MXene/magnetic particles ternary composite to enhance the impedance matching. For example, Liang et al. fabricated a 3D composite aerogel of $\text{Ti}_3\text{C}_2\text{T}_x/\text{RGO}$ anchored by magnetic nickel nanochains for microwave absorption [106]. The directional cell structure and the heterogeneous dielectric/magnetic interface induced perfect impedance matching, multiple polarizations, and electric/magnetic coupling effects, which are favorable for its EM wave absorption performance. The as-prepared ultralight Ni/MXene/RGO aerogel exhibits excellent MA performance with a minimum RL value of -75.2 dB, and the EAB could achieve 7.3 GHz. Further in 2022, Li et al. developed an effective approach to fabricating FeS/MXene/graphene composite aerogels [107]. After the electrostatic self-assembly of MXene on the surface of rGO skeletons, flower-shaped FeS clusters were anchored on the structure through hydrothermal method. The minimum RL value reaches -47.17 dB at a thickness of 4.78 mm, and the maximum EAB can be extended to an unprecedented value of 11.20 GHz.

3.3.4. Polymer/graphene composite aerogel

Conductive polymers are organic polymers that can conduct electricity. Common conductive polymers such as polyacetylene (PA), polypyrrole (PPY), polythiophene (PTh), and polyaniline (PANI) have shown decent electrical conductivity and are used in many fields including electrode materials, photocatalysis, and EMI shielding [108–110]. The combination of conductive polymer with graphene aerogel also induces researchers' interest in recent years for EMI shielding and microwave absorption.

Wu et al. prepared a sponge-like PPY/RGO composite aerogel with an effective absorption band of 6.76 GHz and a minimum RL of -54.4 dB at 12.76 GHz [111]. The SEM images proved that PPY was coated on RGO sheets, resulting in capacitive-like PPY/RGO structures. Under the action of the EM field, a large number of charges will be concentrated in the capacitive structure, which further induces the interfacial polarization and consequently contributes to the attenuation of EM waves. Huangfu et al. fabricated PANI/MWCNT/graphene composite foam via thermal annealing and template-casting method [112]. After the introduction of PANI, the EMI SE value of composite aerogel increased to 43 dB, showing an increase of 16.7% compared with the MWCNT/graphene foam. The authors claimed that the introduction of PANI brought in abundant interfaces, and constructed a more self-contained conductive network, thus enhancing the multiple reflection and the EMI shielding properties immensely. In 2021, Wang et al. proposed an innovative approach to prepare graphene foam/PANI/epoxy (GF/PANI/EP) composites with superior EMI shielding performance as well as thermal/mechanical properties [113]. The graphene foam was first modified by p-phenylenediamine (PPD) to produce the reactive sites for further in-situ polymerization of PANI, and then the epoxy resin is filled in the pores of graphene/PANI composite foam. The SEM images demonstrate a uniform distribution of PANI covered on the graphene sheets, which generates a continuous network. The EMI SE value reached up to 38.32 dB, which are 11 times larger than that of the pristine epoxy matrix. Additionally, the mechanical property and thermal conductivity of composites are also enhanced due to covalent interaction between PANI and graphene.

Besides those conductive polymers, many other insulated polymers

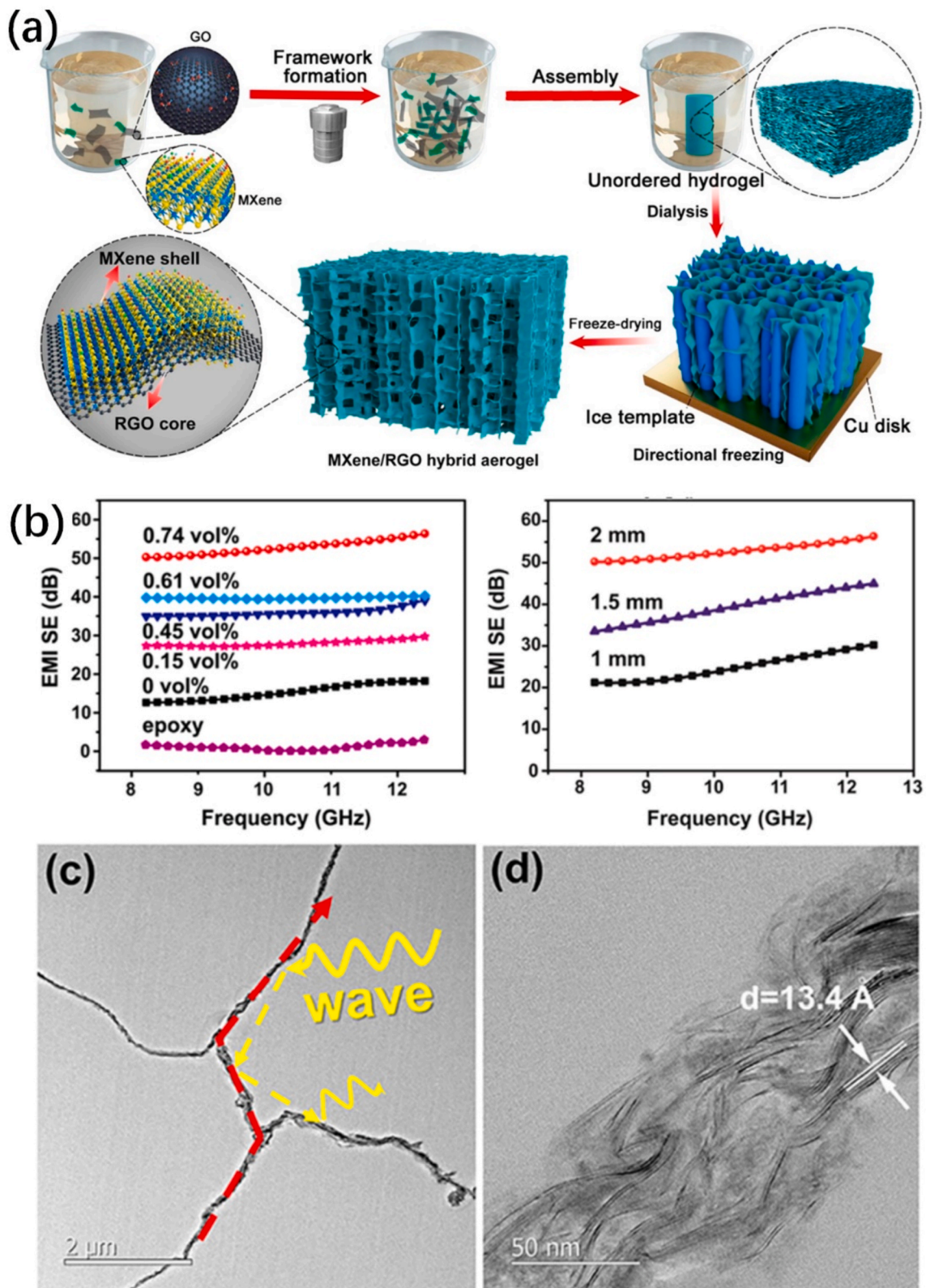


Fig. 12. (a) Fabrication process of MXene/RGO hybrid aerogel by GO-assisted hydrothermal assembly; (b) EMI shielding performances of epoxy/MGA nanocomposites with different content of MXene and the effect of sample thickness on the EMI SE of epoxy/MGA-4 nanocomposite (0.74 vol %); (c, d) TEM images of the epoxy/MGA-4 nanocomposite under different magnifications. Reprinted with permission from Ref. [103].

have also been composited with graphene as aerogel materials, which endow the aerogel with various functions. For example, Li et al. developed a facile foaming route to construct a bubble-template 3D conductive network with graphene and PDMS [114], which exhibited an excellent EMI shielding effectiveness of ~ 86 dB at a thickness of 2 mm. The superior EMI shielding property is ascribed to the abundant close pore structures to reflect and absorb electromagnetic waves, and high electrical conductivity from interconnected 3D graphene networks. Besides, PDMS also facilitates the composite aerogel with flexibility and stretchability. Cheng et al. prepared graphene/polyaramid composite aerogel via solvothermal reaction [115]. The experimental and molecular simulation results demonstrated that aromatic polyaramid could in-situ adhere to the RGO sheets surface during the solvothermal reaction, which is derived from the high density interfacial π - π interactions between RGO and benzene rings of polyaramid. More interestingly, this adhered thermal-resistant polyaramid could also act as the anti-oxidation barrier layer for RGO aerogel, endowing it with stable microwave absorption performance at high temperature. The aerogel's EM wave absorption performance could be completely preserved after 300 °C treatment in air atmosphere. Furthermore, the composite aerogel also exhibits multi-functions, including good compressive performance, thermal-insulating and flame-retardance.

3.3.5. Metal-organic frameworks (MOF)/graphene composite aerogel

Recently, MOFs have attracted tremendous attention owing to their tunable chemical structures, diverse properties, large specific surface area, and porous morphology, which have been adapted as EM functional materials by many researchers [116–118]. MOF could be transformed to porous carbon with the decoration of metal oxides at high temperatures, thus endowing it with simultaneous dielectric and magnetic loss for microwave dissipations. Besides, the compositing of MOFs with other nanomaterial is also hugely studied, and graphene aerogel is one of the most important with excellent performance [119,120]. In 2020, Liu et al. prepared γ -Fe₂O₃/C/RGO composite material by the facile hydrothermal method of MIL-53 MOF, combined with the calcination process [121]. Through appropriate doping ratio and calcination temperature, the minimum RL value can achieve -43.13 dB, with an excellent EAB of 11.68 GHz. In 2021, Zhang et al. fabricated a CoTe₂ MOF/GO composite aerogel via the solvothermal method [122]. The resultant MOF-derivative CoTe₂ exhibit nano porous structures, with pore diameters ranging from 1 to 10 μ m, which is also uniformly distributed on the RGO sheet inside the skeleton. The unique microstructure and dielectric/magnetic component provide the aerogel with excellent microwave absorption performance in both GHz and THz band. Specifically, the optimal RL was up to -62.2 dB at 13.04 GHz, and the EAB is 8.2 GHz in GHz band. The excellent EM wave absorption performance should be derived from the following three aspects. First, the porous RGO forms a continuous conductive network, which could attenuate the microwave by multiple reflection and scattering, and dissipate the energy into microcurrent and heat. Secondly, the CoTe₂ can enhance multi-interfacial polarization with numerous interfaces between CoTe₂ and RGO sheets, and the CoTe₂ also provide dielectric loss due to its electrically conductive properties. Thirdly, the natural resonance and eddy current losses are generated by ferromagnetic Co nanoparticles.

Apart from the solvothermal reaction, the MOF/graphene aerogel could be also generated by the coordination/electrostatic interaction of metal ions and GO. In 2022, Huang et al. prepared MOF/RGO aerogels based on the gelation of GO, which is directly initiated using MOF crystals [123]. The metal ions from MOF act as the crosslinkers for GO sheets to form a stable 3D porous nanonetwork via metal-oxygen electrostatic interactions. The further thermal treatment has transformed the MOF/GO structure to Fe₃O₄@C/RGO magnetic/dielectric hybrid aerogels (Fig. 13a/b). Typically, it presents a highly porous 3D structure of RGO crosslinking (Fig. 13c/d). The synergistic effects of magnetic/dielectric performance and porous structure provide the aerogel with

notable microwave absorption performance with strong absorption (-58.1 dB) and broad bandwidth (6.48 GHz) at low thickness (2.5 mm) (Fig. 13e).

3.3.6. Carbon material/graphene composite aerogel

Similar to metal/graphene composite aerogel, the application of carbon/graphene composite aerogel is beneficial to EMI shielding and microwave absorption because of the high conductivity of carbon-based materials, such as carbon nanotubes, carbon fibers, and fullerene, etc [51,124–126]. Zhao et al. reported PDMS/RGO/single-wall carbon nanotube (SWCNT) nanocomposite as EMI shielding materials [127]. The RGO/SWCNT conducting network was firstly constructed and then backfilled with flexible PDMS matrix. The incorporation of SWCNT obviously improved the intrinsically high conductivity of composites. The interconnected RGO/SWCNT interconnected 3D network could serve as fast channel for electron transport, and induced an outstanding EMI SE value of 31 dB in the X band. Chen et al. prepared a multiwalled carbon nanotube (MWCNT)/RGO foam via a self-assembly solvothermal method and thermal reduction [128]. Compared with RGO foam, the composite aerogel possesses a larger pore size and a more regular and complete pore wall structure, and this should be owing to the reinforcement effect of MWCNT. With the increase of MWCNT content and annealing temperature, the electrical conductivity of composite aerogel gradually increases, which presents an efficient method for the regulation of aerogel's electromagnetic properties. Due to the interlaced network of MWCNT, the optimized EM absorption performance could achieve the entire qualified bandwidth of 16 GHz (2–18 GHz) and a minimum RL value of -39.5 dB, which is superior to most literatures. Recently, Cao et al. also provided carbon fiber/RGO aerogel fabricated by a similar solvothermal reaction [129]. Compared with RGO sheets, carbon fiber displayed an obviously larger size, with a length of 1–2 mm. Therefore, T1000 carbon fibers are interspersed inside the pore of aerogel, rather than adhering to the graphene sheets as pore walls. Compared with that of pure RGO aerogel, the complex permittivity values were nearly doubled in the 2–18 GHz band with the addition of 100 wt% carbon fiber, and this is obviously attributed to the high conductivity of carbon fibers. By regulating the annealing temperatures of composite aerogel, an optimal EAB value of 8.72 GHz was obtained in 2–18 GHz. Besides, the compressible composite aerogel also demonstrates superior and stable EMI shielding performance under in-situ compression. The EMI shielding effectiveness exceeds 35 dB in the X band with a compression ratio of 78.9% at the thickness of 4 mm. Graphyne is a kind of new carbon material composed of sp and sp²-hybridized carbon atoms, and it has displayed various application aspects in the field of energy storage, photocatalytic reactions [130–132]. Zhang et al. firstly fabricated the γ -Graphyne(γ -GY)/RGO composite aerogel by the solvothermal self-assembly [133]. The γ -GY was firstly synthesized using a mechanochemical ball-milling method. Then it went through the facile solvothermal reaction with GO solution. The minimum RL value of composite aerogel is -71.73 dB at 10.48 GHz, and the EAB value could reach 7.36 GHz. Additionally, excellent THz absorption property is also obtained at 0.2–1.6 THz.

Besides those regular synthesized carbon materials, carbon-based material could be also fabricated by thermal annealing of polymers, such as the carbonization of polyimide and epoxy resin. Various polymers have been compensated with graphene to prepare the foam/aerogel materials, and the pyrolyzed sample was transformed to carbon/graphene composite aerogel. Song et al. [134] prepared a cellulose carbon aerogel (CCA)/RGO aerogel using vacuum impregnation, and freeze-drying followed by thermal annealing methods. The cellulose precursor forms carbon fiber after the thermal annealing, and two different conductive networks (CCA and RGO) were simultaneously generated inside the composites. These two conductive networks work together to form a perfect 3D double-layer network for effective microwave dissipation, which significantly improves the EMI SE (51 dB) of composite aerogel.

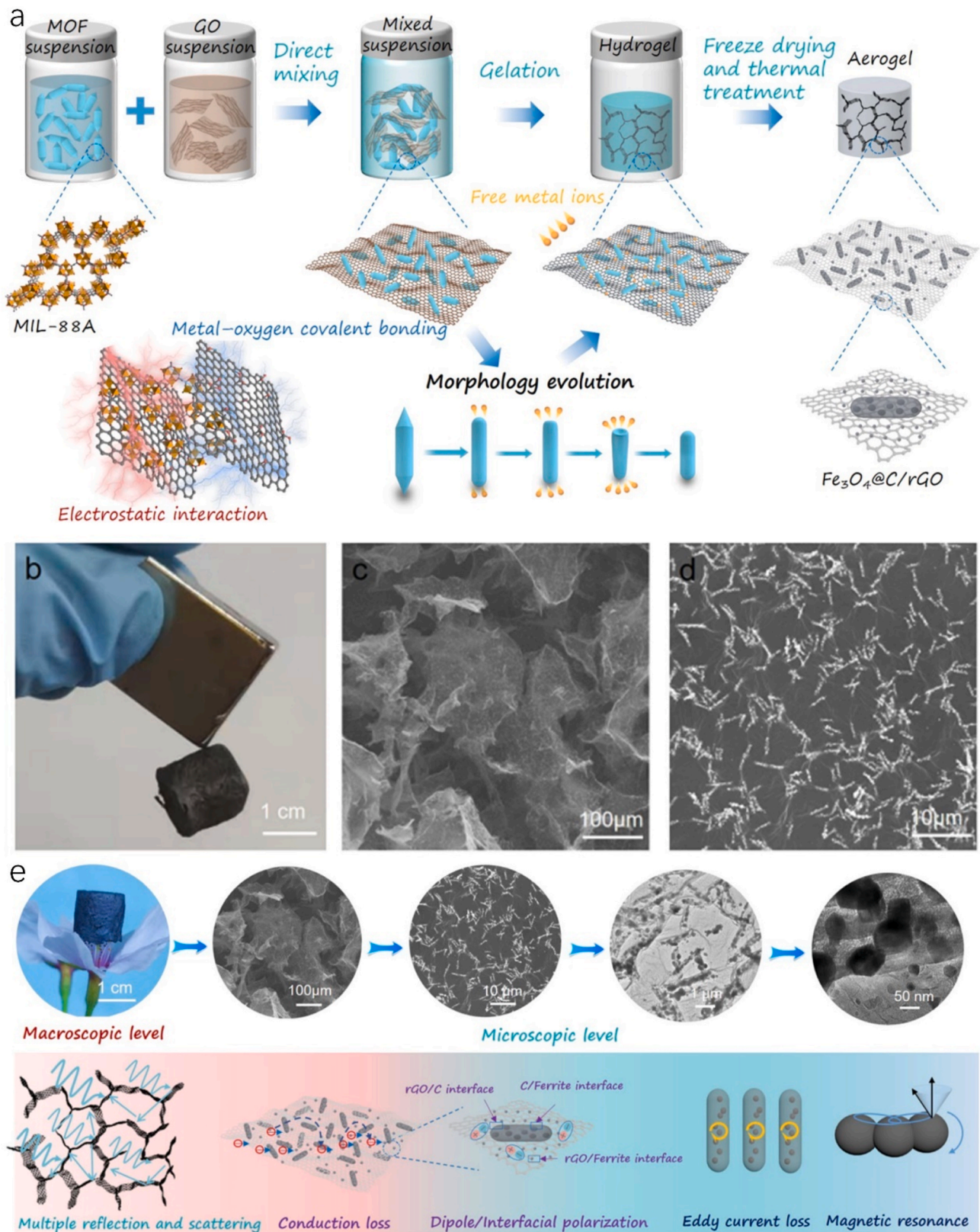


Fig. 13. (a) Schematic of the fabrication process of MOF/RGO hybrid aerogels; (b) optical images of aerogel encountering magnet; (c–d) SEM images of composite aerogel; (e) schematic of the associated microwave absorption mechanism of the proposed MOF/RGO-derived magnetic and dielectric aerogels. Reprinted with permission from Ref. [123].

3.3.7. Comparison of graphene aerogels and its composites as EMI shielding materials

As have been mentioned, various graphene aerogels and their composites have been developed as EMI shielding materials. Their EMI shielding performance and corresponding materials type are summarized as followed in Table 1. As can be seen, those doped graphene aerogels, and metal/graphene composite aerogels own high EMI SE values, and some of them are higher than 80 dB. This is mainly derived from their highly improved electrical conductivities, compared with

Table 1
The EMI shielding performance of different kinds of graphene aerogel materials.

Type	Materials	EMI SE (dB)	Frequency band (GHz)	Thickness (mm)	Refs.
Pure graphene aerogel	Graphene aerogel prepared by Vitamin C reduction	30.9	8.2–12.4	2.5	[11]
	RGO aerogel prepared by CVD method	135	0.1–3	1.4	[12]
	RGO aerogel prepared by high-temperature treatment	20	8.2–12.4	1	[81]
Metal/graphene composite aerogel	Ni-chains/RGO microcellular foam	40.82	8.2–12.4	2	[90]
	silver plates/RGO foams	58	8.2–12.4	3	[91]
	Ag NW/graphene foam	84.01	8.2–12.4	4	[92]
Magnetic material/graphene aerogel	graphene/Fe ₃ O ₄ /PDMS composite aerogels	70.37	8.2–12.4	2	[94]
	Fe ₃ O ₄ /graphene foam	32.4	8.2–12.4	1	[95]
	YIG-graphene aerogel/buckypaper metacomposite	70	8.2–12.4	4	[97]
MXene/graphene composite aerogel	Ti ₃ C ₂ T _x /GO composite aerogel	50.7	8.2–12.4	1.5	[135]
	MXene/graphene/polymer composite	43.3	8.2–12.4	2.4	[105]
Conductive polymer/graphene composite aerogel	PANI/MWCNT/graphene composite foam	43	8.2–12.4	3	[112]
	graphene foam/PANI/epoxy	38.32	8.2–12.4	4	[113]
Carbon material/graphene composite aerogel	RGO/SWCNT composites	31	8.2–12.4	2	[127]
	Carbon fiber/RGO aerogel	51.6	8.2–12.4	19	[129]
	cellulose carbon aerogel/RGO aerogel composites	51	8.2–12.4	10	[134]
Heteroatom doped graphene aerogel	N doped carbon aerogel by biomass pyrolysis	82	8.2–12.4	13	[136]
	N, S-co-doped TiC/carbon hybrid aerogel	80	8.2–12.4	2	[137]
MOF/graphene composite aerogel	ZIF-8 derived material/graphene aerogel	48	8.2–12.4	1	[138]

pure graphene aerogel. However, their corresponding EMI shielding mechanisms are mostly reflection-dominated rather than absorption-dominated, which would generate secondary pollution. Instead, a large proportion of the composite aerogels, such as the polymer/graphene aerogel, ferrites/graphene aerogel, MOF-graphene aerogels, display a moderate EMI SE values, which are mostly in the range of 20–50 dB. Nevertheless, their EMI shielding mechanisms are mainly absorption-dominated, since those materials possess low electrical conductivity or even are insulators. In this case, the overall electrical conductivities are similar with the RGO aerogel, and the EM waves tends to incident insides the aerogel and further been attenuated.

To further illustrate the unique absorption-dominated EMI shielding properties of graphene aerogels, we also summarized the absorption coefficient (A), reflectivity coefficient (R) of those graphene composite aerogels, and the special A/R values are also calculated to verify their main shielding mechanisms. As shown in Table 2, the A/R values of those graphene composite aerogels are all higher than 1, and this demonstrated that the absorption ratio for EM waves are higher than the reflection, which once again proved their absorption-dominated EMI shielding performance. For comparison, the A, R and A/R values of some heavily-researched EMI shielding materials, such as MXene aerogel/films, graphene films and metal foams, are also presented. Although they may possess high EMI SE values, their A/R value are all below 1, and some of them are even lower than 0.1, which proves them as reflection-dominated EMI shielding materials. The huge differences of graphene composite aerogels with them are mainly derived from the following two parts. Firstly, those reflection-dominated EMI shielding materials, such as MXene aerogels/films and graphene films, usually possess high electrical conductivity (most of them are higher than 10⁶ S/m), and their impedance matching properties are obviously weak, so that EM waves tends to reflect once they incident with these materials. While for those graphene composite aerogels, their electrical conductivities are lower, and the incorporation of those conductive polymers or ferrites also benefits the impedance matching degree, so the reflectivity coefficient of EM waves are significantly reduced. Secondly, these graphene-based composite aerogels usually have multiple loss mechanism, such as interfacial polarization, eddy current loss, which would greatly enhance the attenuation of microwaves. Besides, the porous structure of aerogels also promotes multiple reflection and scattering of EM waves inside the aerogel, and this further contributed to EM waves' dissipation and improves the absorption coefficient. Therefore, those graphene-based composite aerogels are promising EMI shielding materials with absorption-dominated shielding effects, which could be

Table 2
The comparison of EMI shielding performance and their detail R, A values of graphen composite aerogel with other heavily-researched EMI shielding materials.

Type	A	R	A/R value	EMI SE (dB)	σ (S/m)	Refs.
Graphene composite aerogels	0.66	0.33	2	20	5	[139]
	0.55	0.44	1.24	27.6	50	[140]
	0.72	0.26	2.76	12	26.5	[92]
	0.8	0.10	8	10	8.2	[141]
	0.69	0.3	2.3	97.3	749.2	[142]
MXene aerogels	0.6	0.39	1.54	32	18.39	[143]
	0.82	0.14	5.85	13	< 0.5	[42]
	0–0.1	0.9–1	< 0.11	70	> 50	[144]
	0.1–0.2	0.8–0.9	< 0.25	80	> 1400	[145]
	0.15–0.2	0.8–0.85	< 0.25	20	437	[146]
MXene films	0.044	0.955	0.046	46.1	1150000	[147]
	0–0.05	0.95–1	<	75	181900	[148]
Graphene films			0.053			
	0–0.1	0.9–1	< 0.11	70	1633.6	[149]
Metal aerogels	0–0.061	0.939	<	93.8	1582	[150]
	0.1–0.15	0.85–0.9	< 0.67	70.1	363.1	[151]

applied in various fields including consumer electronics, automotive electronics, etc.

4. Smart and multi-functional EMI shielding materials based on graphene aerogel

Making equipment smart and multifunctions-integrated is irreversible trend for EM functional materials. The EMI shielding/microwave absorption performances of graphene aerogels intrinsically originate from their electrical/polarization behavior, which could be tuned by various external stimulus, such as mechanical compression, and thermal/electrical excitations (Fig. 14a–b). Therefore, graphene aerogels could be regarded as smart EM functional materials to some extent. What is more, the aerogel structure and graphene's intrinsic properties also provide graphene aerogel with various functions, including strain sensing, thermal insulation (Fig. 14c–f). The detail mechanisms and examples are presented as follows.

4.1. Smart graphene-based aerogel for EMI shielding

4.1.1. Compressive-stimuli for its EMI shielding property

Graphene aerogels are well known for their large-scale, repeatable compressive performance, and this presents great influences on their EMI shielding properties, thus making them smart EMI shielding materials. Zhang et al. firstly discovered the compression effects for graphene aerogels' microwave absorption performance in 2015 [82]. Compared with the pristine aerogel, the compressed aerogel shows an enhanced dielectric loss in 2–18 GHz, which is closely associated with the 3D structure transforming during compression. The void space shrinking leads to more physical contacts between conductive graphene sheets,

therefore increasing the resonance circuit density. In 2020, Li et al. systematically studied the changes of microwave reflection, absorption, and shielding when graphene aerogels are compressed with different strains [11]. It is found that there is no significant difference in its EMI shielding performance with low compression strains (0–40%). With strain increasing to 60%, the EMI shielding performance improves from 15 dB to 31 dB. The improvement of its shielding effectiveness is mainly attributed to its improved electrical conductivity. Generally, the compression induces closer contact of graphene sheets inside the aerogels, thus providing more electron transport channels and higher dissipation ability towards microwaves.

Although the EMI shielding performance could be in-situ regulated by compression for graphene aerogel, the change degree is rather limited, and hinders its application as smart EM devices. Recently, Liu et al. reported an off/on switchable EMI shielding material composed of graphene aerogel filled with conductive carbon nanoparticles [152]. The original aerogel possesses low dielectric loss and microwaves are mostly transmitted, with an EMI SE of only 1.4 dB. While after the compression, the decorated carbon nanoparticles have established high conductive pathways inside the aerogel, and significantly increase the conductivity of the aerogel, thus activating its EMI shielding performance to 27.6 dB (Fig. 15a–f). Such an off/on switchable EMI shielding materials have great potential in advanced smart and multifunctional EM response systems in the future.

4.1.2. Thermal-stimuli for its EMI shielding property

Besides the mechanical response, the thermal response for EMI shielding properties of graphene aerogel, especially the RGO aerogel has attracted researchers' attention. Cao's group has long been devoted to studying the temperature responded EM performance of carbon-based

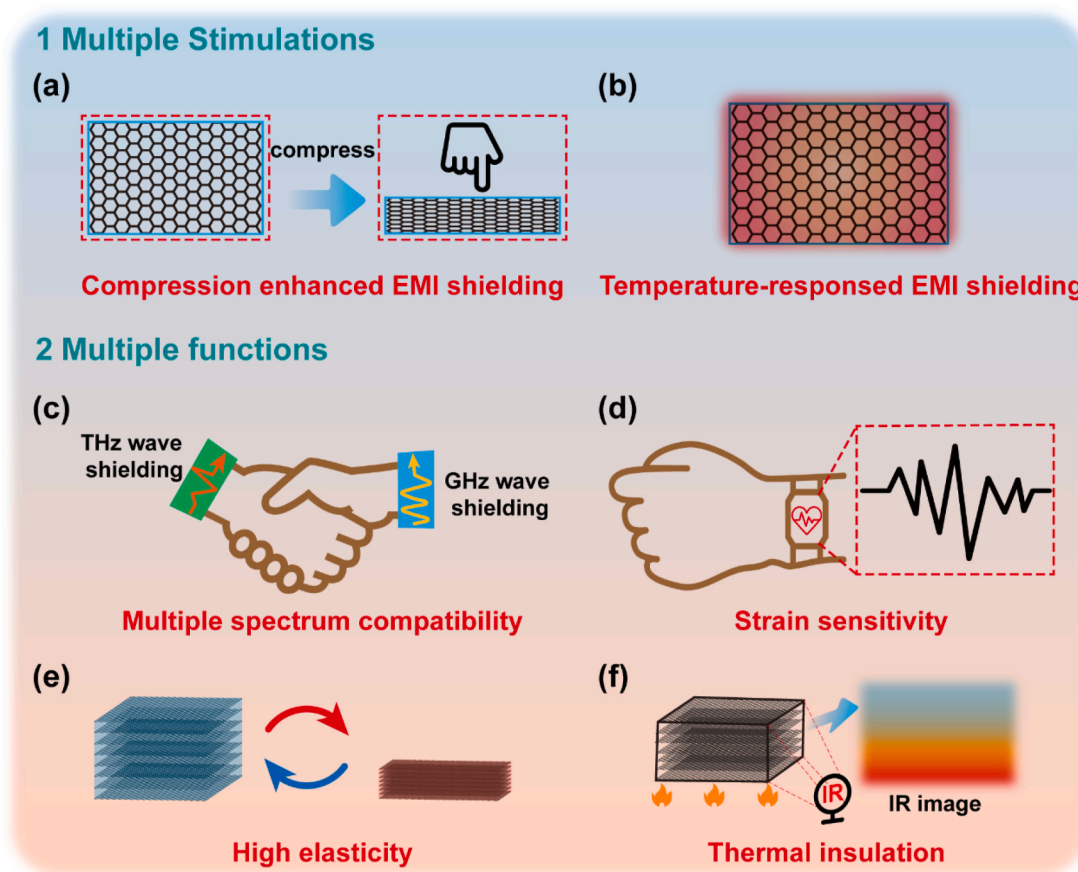


Fig. 14. (a/b) multiple-stimulus of graphene aerogel as smart EMI shielding materials; multiple function of graphene aerogel such as (c) multiple band compatibility, (d) strain sensing, (e) high elasticity, and (f) thermal insulation.

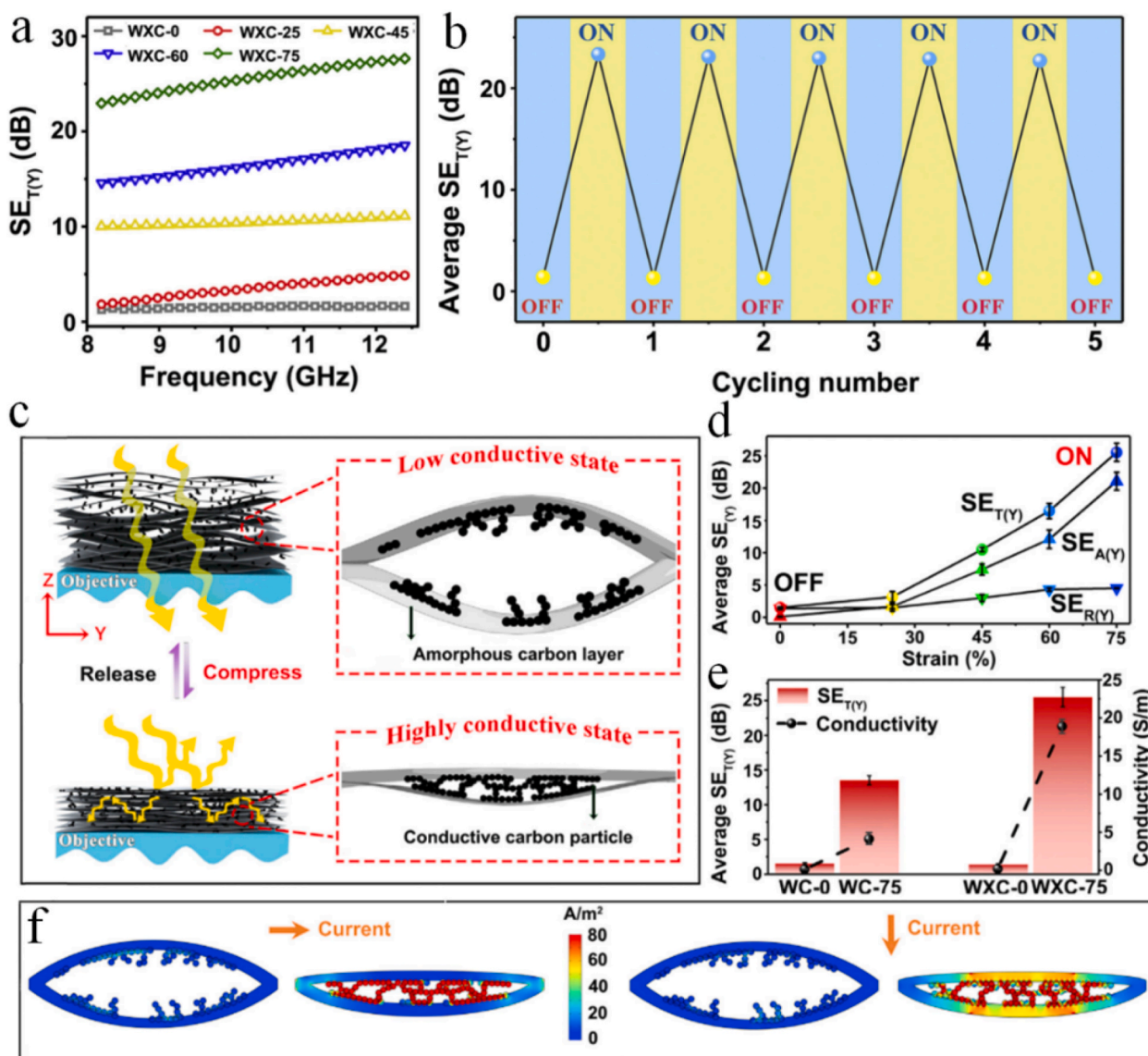


Fig. 15. (a) SE_T of the graphene/carbon nanoparticles aerogel with different compressive strains; (b) cyclicality of “off” and “on” states of EMI shielding for the composite aerogel; (c) schematic illustration of the off/on shielding performance of the switchable EMI; (d) variations of average $SE_T(Y)$, $SE_A(Y)$, and $SE_R(Y)$ with compressive strain; (e) comparison of average $SE_T(Y)$ and Y-directional conductivity of composite aerogels before and after compression; (f) simulation of current density in 2D structure. The arrows indicate the current directions (from left to right and from top to bottom). Reprinted with permission from Ref. [152].

nano materials, such as graphene and carbon nanotubes [153–156]. The temperature-dependent microwave absorption performance of RGO composites was firstly reported in 2014 [157], and both dipole polarization and hopping conductivity of RGO sheets have been evaluated, and show strong impacts on their EMI shielding performance. In 2021, his group further synthesized Fe_3O_4 /RGO aerogel composites [158], and the microwave absorption response to temperature is discussed in detail. The results demonstrated that increasing temperature makes changes to the electromagnetic parameters of composites. For composites with low loadings (12 wt%), the polarization behavior dominates the dielectric loss of this loosely connected structure, and the ϵ'' of hybrid composites drops when the temperature rises from 323 to 523 K, since the high temperature restrains the relaxation process. With high loading of composites (28 wt%) in which a conductive network is successfully constructed, the ϵ'' is positive correlated with temperature, due to the enhancement in electron transport by heat excitation. However, the improvements for ϵ'' of these aerogel composites are not that conspicuous in this temperature range, leading to limited changes in its EMI shielding/microwave absorption performance.

Recently, Cheng et al. reported an intelligent temperature-responded microwave absorption material based on RGO/ VO_2 composite aerogel [159]. The composite aerogel demonstrated off/on switchable MA performance, which originated from the unique phase change behavior of VO_2 (Fig. 16a). As temperature increases (>68 °C), the VO_2 inside the aerogel displays the phase change behavior, which accompanies with significant changes in aerogel permittivity, and consequently leads to off/on switchable MA performance. The maximum changes for the effective absorption bands (ΔEAB) and RL values (ΔRL) can be as high as 7.27 GHz and 49 dB (Fig. 16b/c), which exceeds most reports, and the off/on switch behavior is demonstrated to have good cyclic stability.

Smart responsive polymer materials are polymers that are highly responsive to external stimulus, and they have been hugely investigated by researchers. The introduction of those smart responsive polymer materials into graphene aerogel may endow the composites with smart properties, which may realize the in-situ regulation of EM waves' transmission/absorption/reflection. Inspired by this, poly(N-isopropylacrylamide) (PNIPAAm), a temperature-responsive polymer, was composited with graphene aerogel [160]. The macromolecular

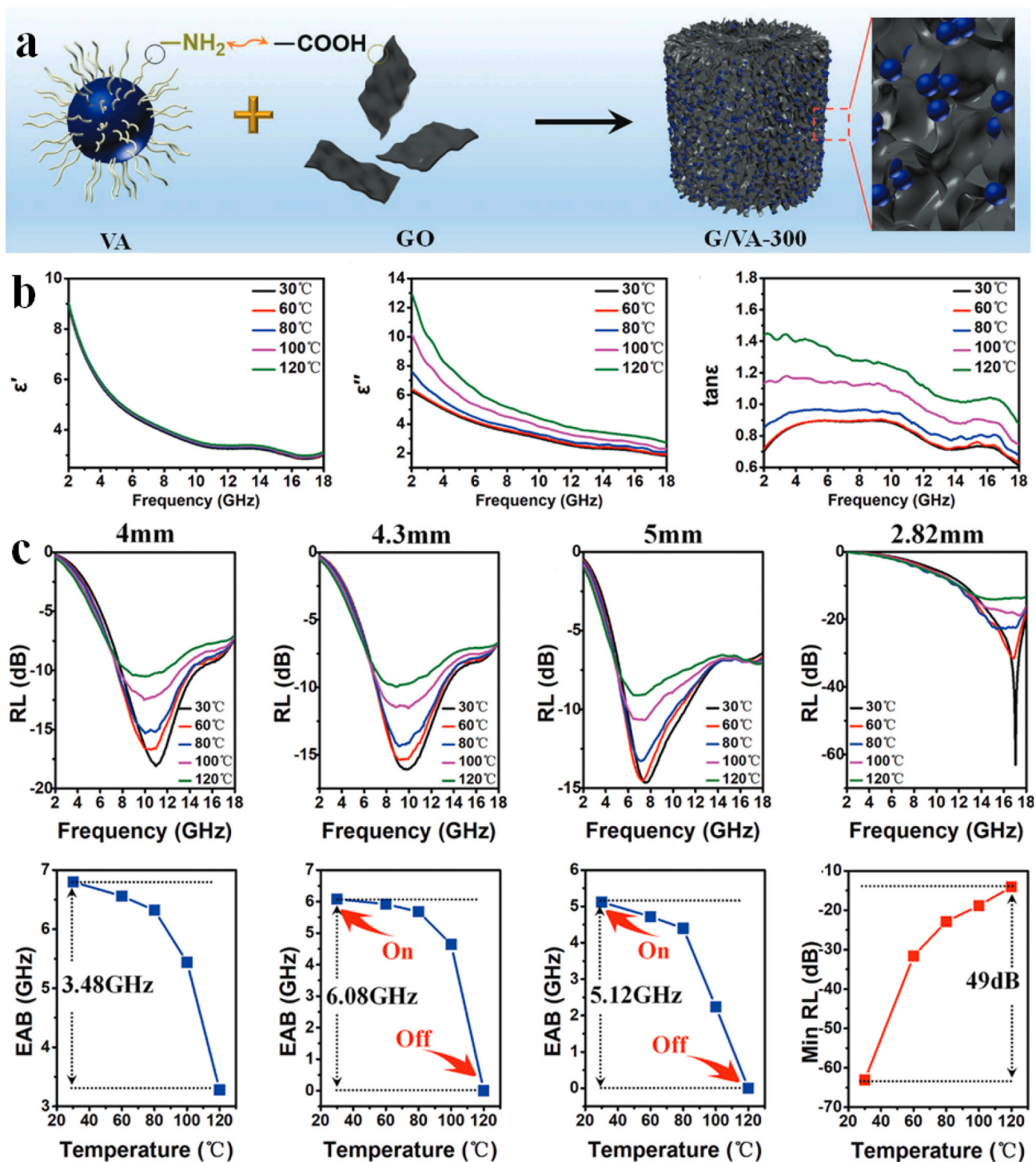


Fig. 16. (a) Schematic illustration for the fabrication process of rGO/VO₂ composites; (b) the temperature-dependent complex permittivity for RGO/VO₂ composite aerogel; (c) the temperature-dependent MA performance and corresponding EAB values of G/VA-300 at 4 mm, 4.3 mm and 5 mm, minimum RL values at 2.82 mm. Reprinted with permission from Ref. [159].

conformation of PNIPAAm could be dynamically changed with a critical temperature of 34.8 °C, due to the intramolecular hydrogen-bonding interactions eliminating and reforming. This drives the RGO sheets in composites aerogel to delaminate and restack as temperature changes, further leading to the smart temperature responded microwave absorption performance. As temperature increases from 20 to 50 °C, the absorption band range could be tuned from 8.5–17.5 GHz to 4.5–14.0 GHz.

4.2. Multi-functional graphene aerogel-based EMI shielding materials

4.2.1. Graphene aerogel-based multiple-bands shielding materials

Nowadays, the research on the EMI shielding materials is mainly concentrated in the microwave frequency, due to its wide application in various fields, such as 5G and radar detection. Recently, THz wave has become the new frontier for photonics owing to its potential applications in data transmission, high-resolution imaging, and radar detection. As the intermediate band between microwave and infrared light, THz

frequency range (wavelengths of 30 microns–1 mm) is distinct from the conventional microwave range, which is centered around wavelengths of a few centimeters. Several countries have devoted huge energies to THz wave technology for the development of 6G wireless communication, since it could transmit more information with a higher internet speed and lower latency, compared with the 5G technology. This has fueled unprecedented growth in the development of THz devices, circuits, and THz-based communication systems. Correspondingly, EM functional materials with THz shielding properties have received more and more attention from researchers.

Graphene has been demonstrated as THz-response material, mainly owing to its electro-conductive properties, which are responsible for reflecting THz waves. Rodríguez et al. have measured the transmittance of THz wave for single/multiple-layer graphene [161]. In the 0.57–0.63 THz range, single-layer graphene on SiC showed a transmittance of ~ 0.8 (SE ~ 0.97 dB). A two-layer graphene film gave a transmittance of roughly 0.7 (SE of 1.54 dB), which both shows great shielding effects of graphene to THz waves. As for these graphene derivatives, such as GO and RGO, the researches are also in its swing. In 2013, Hong et al. measured the THz conductivity and refractive indexes of RGO films using the Drude free-electron model [162]. It demonstrated that the THz conductivities can be manipulated by controlling the thermal reduction

process, similar to that of EMI shielding performance in the microwave range. In 2017, Huang et al. firstly reported ultra-broadband wide-angle THz absorption properties of 3D RGO foam with a porosity of 99.9% and density of 0.80 mg/cm^3 [83]. The porous structure of RGO foam with a low dielectric constant significantly facilitates the low surface reflection of THz waves, which is rather different from the shielding mechanism of pure graphene films. Besides, the effects of annealing temperature were also carefully evaluated. The foam annealed at 1000°C possesses a THz absorption performance with a maximum RL value of 19 dB and qualified frequency bandwidth of 1.045 THz. In addition, it is found that the THz absorptivity was obviously increased with the incident angle increasing, and this is derived from the longer optical distance and larger surface scattering. In view of excellent THz and GHz absorption, graphene aerogel could be considered as a compatible GHz/THz absorption/shielding material suitable for future 6G communication devices and terminal equipment. Following this, a series of graphene based composite aerogels have been fabricated as THz absorption/shielding materials, including RGO/polyaramid aerogel [115], RGO/Co-MOF aerogel [122], RGO/MXene aerogel [104], and RGO/ Fe_3O_4 aerogel [163]. For example, the carbon fiber/RGO composite aerogel demonstrated an average SE value of 34.0 dB in the THz band with a density of only 3.75 mg/cm^3 [129]. The RGO@Co-MOF

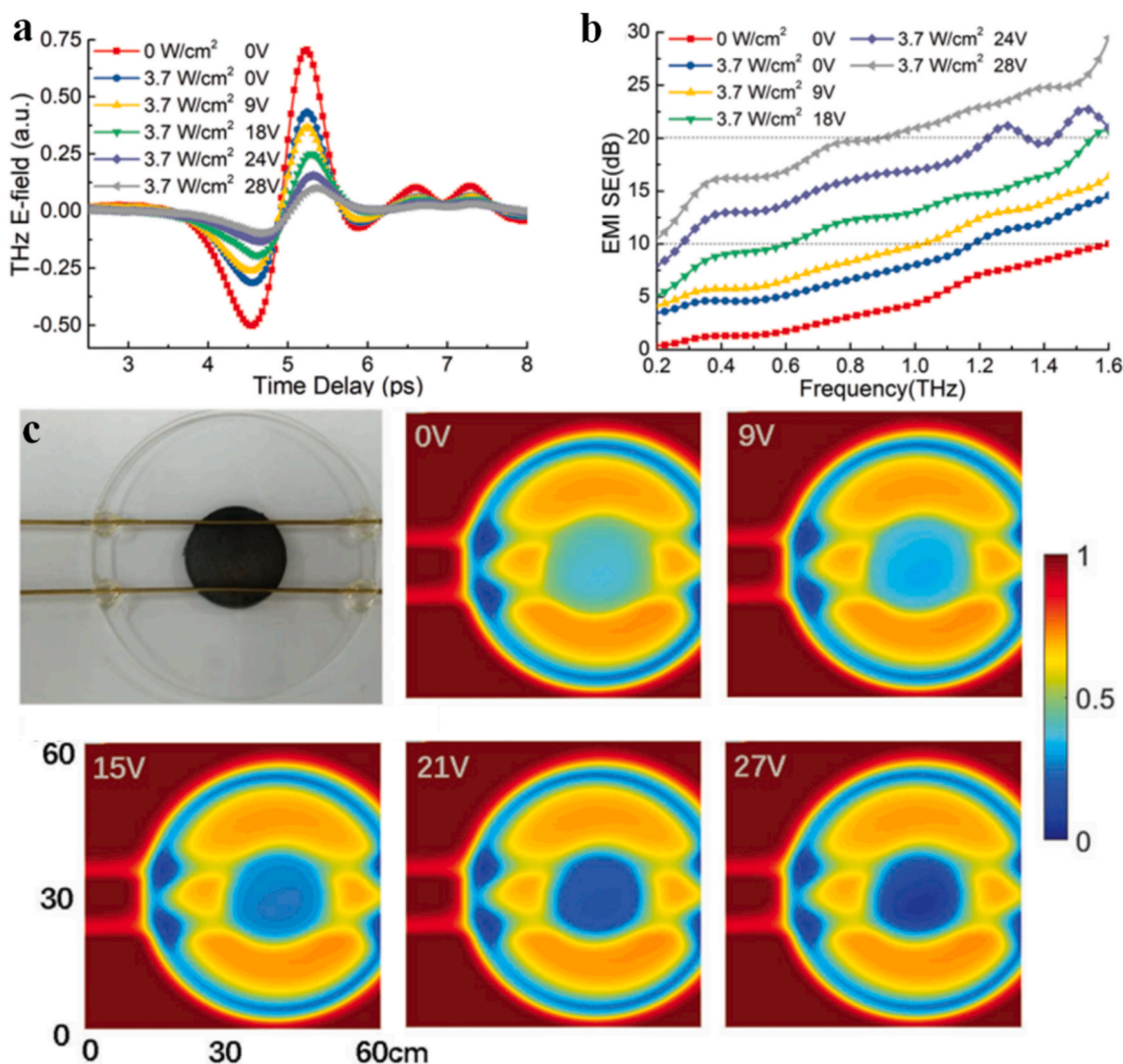


Fig. 17. (a) Experimental THz-TDS signals of tunable GF controlled by both optical and electrical field excitations, the voltages of the electrical field are increased from 0 to 28 V, and meanwhile the laser excitations of a 3.7 W cm^{-1} are applied and (b) their corresponding EMI SE curves; (c) THz transmission imaging of RGO foam with different voltages. Reprinted with permission from Ref. [164].

composites show the maximum RL value of 54.07 dB, which covers the entire bandwidth from 0.2 to 2 THz [122].

Moreover, the activation of THz absorption/shielding by outer stimuli has also attracted people's attention. Xu et al. modulated the THz response of RGO foam via both bias electric field and laser pumping [164]. The RGO foam can be tuned from off-shielding state to on-shielding state when external field excitation is applied (Fig. 17a/b), and this is mainly resulted from the absorption changes, which is also verified by the THz transmission imaging (Fig. 17c). The modulation mechanism demonstrated that the nonequilibrium carriers can be generated via bias electric field, so the Fermi level will be raised to a higher conduction band, which finally enhanced its absorption in the THz band.

4.2.2. Graphene aerogel EMI shielding materials with strain-sensing property

Due to the improved density and additional conductive paths, the electrical resistance of 3D structured graphene decreases upon mechanical compression, making them promising materials as pressure sensors. Recently, multi-functional graphene aerogel has been reported with simultaneous EMI shielding and strain sensing performance [165–167]. Nguyen et al. reported a graphene/Fe₃O₄/MXene foam reinforced by PDMS [168]. The composite exhibits excellent EMI SE of 80 dB in the X band and 77 dB in the Ku band owing to the excellent microwave absorption performance. What is more, it also presents good pressure-sensing properties due to the large surface area, good elasticity, and rapid recovery. The pressure value from 62.4 to 998.9 kPa was monitored for its sensing performance, with long-term stability in 4000 cycles. These results indicate that the composite could be used as potential artificial EMI shielding skin for human emotion recognition. In 2021, Xu et al. prepared honeycomb porous graphene by laser scribing technology, and the honeycomb structure provides the material with an EMI SE up to 45 dB with a thickness of 48.3 μm [169]. Moreover, the porous material also exhibits durability in cyclic stretching and bending, and thus could be used to monitor weak physiological signals such as pulse, respiration, and laryngeal movement of humans. In 2022, Xu et al. further fabricated lightweight and stretchable graphene armor for EMI shielding and strain sensing [165]. The graphene armor is composed of laminated graphene film (LGF) and hierarchical porous graphene foam (HGF) with film/foam/film sandwich architecture, which displays great EMI shielding performance with low thickness. Due to the LGF being firmly embedded in the rough surface of the HGF, the cracks of the LGF will move along with the HGF without falling when the tensile strain of sandwich graphene armor occurs. This provides an effective approach to improving the sensitivity of strain sensors with the highest gauge factor of 258. It is believed that such multifunctional materials with both EMI shielding and human physiological signal monitoring would create more potential for the next generation of wearable electronic devices.

4.2.3. High elastic graphene aerogel as EMI shielding materials

Although graphene aerogel has demonstrated various advantages, including good electrical conductivity, high porosity, low density, and large specific surface area, its application in practical environment is still restrained by its weak mechanical performance, and it remains a challenge to construct graphene-based aerogels with high strength and elasticity. Considering its porous structure, the overall compressive strength/modulus could not be compared with those densely-packed materials, such as films, fibers, and metals. However, graphene aerogels could be constructed with high elasticity, which means that it could withstand large-scale compression and maintain its original shape for hundreds of times or even thousands of times, and this will greatly enhance its practical application value as EMI shielding materials. Generally, the mechanical performance of aerogels relies on their cellular architecture, density, constituted components, and bonding patterns. Since 2015, there have existed two main strategies to enhance the compression properties of graphene aerogel. The first is the

compositing with other materials for mechanical enhancements, such as polymers [170], carbon nanofibers [171], and MWCNTs [172]. For example, a series of cellulose fiber/RGO aerogels were prepared by Wan et al. [41]. The one-dimensional cellulose fiber serves as the skeleton for the aerogel, and the compressive stress only shows a decrease of 5–20% at 50% strain for 10 cycles. Zeng et al. reported the highly elastic graphene/lignin-derived carbon aerogels with high EMI shielding performance [173]. The aligned porous architectures of composite aerogel were constructed by ice-templated method, using a bottom cold source, and this finally endow it with anisotropic mechanical performance. It shows complete recovery and excellent reversibility after the compressive process with strains even up to 70% in transverse direction. The second strategy is defects-repairing of graphene aerogels by gluing individual graphene sheets with stronger contacts for the aerogel. Wang et al. found that crosslinks of graphene sheets are the key factors responsible for its elasticity by molecular simulations [174], and this further guided the researchers for the improvement of graphene aerogel's elasticity. For example, an interfacial reinforcement approach is proposed to reinforce graphene networks by incorporating graphitized polyimide carbon [175]. The polyimide component is graphitized to carbon to bridge the graphene sheets, resulting in an integrated graphene aerogel with satisfactory mechanical and functional performances. The composites achieved reliable resistance to fatigue, with a negligible plastic volume deformation (~2%) and retains 90% of the maximal stress after 1000 cycles of fast compression at 50% strain.

4.2.4. Thermal-insulated graphene aerogel as EMI shielding materials

Graphene aerogels are highly filled with air inside, with a porosity over 99%, making them ideal candidates for thermal insulation applications. Therefore, various bi-functional graphene aerogels with both EMI shielding and thermal insulation properties are synthesized [115, 129]. Jiang et al. prepared a series of anisotropic graphene/carbon aerogels by the carbonization of graphene/PI aerogels [176]. The unidirectional freezing method provides it with anisotropic characters. The thermal conductivity in the axial direction (graphene sheet oriented) was much higher than that of its radial direction, due to the well-constructed graphene/carbon wall for heat transfer. The radial thermal conductivity was as low as 0.038 W m⁻¹ K⁻¹, while that of the axial direction is 0.196 W m⁻¹ K⁻¹. Therefore, the radial direction owns better thermal insulation performance. When placed on a hot plate, the temperature rise in the radial direction are always lower than that in the axial direction. Moreover, the fabricated composite aerogel also possesses good EMI shielding performance, with highest EMI SE value of 54.1 dB with a thickness of 2 mm. In 2022, Chen et al. [177] reported a honeycomb-like graphene anisotropic aerogel by assembling the hollow porous RGO in a macrotubes array structure, followed by the encapsulation of PDMS (Fig. 18a). When placed on a hot table (~150 °C), the axial sample displayed an obviously higher temperature than that of the radial sample (Fig. 18b), due to their different thermal conductivity in different directions. Besides, the composites aerogel also exhibited good EMI shielding performance in response to compression strains (Fig. 18c).

5. Conclusion and outlook

In general, graphene aerogels have been proven to have excellent EMI shielding properties after years of development. Unlike reflection-dominated shielding materials (such as metals), most graphene aerogels present the absorption-dominated EMI shielding mechanism, which makes them more suitable to reduce secondary EM pollution. In terms of their preparation, various methods have been proposed, and endow the graphene aerogels with different structures and electromagnetic properties. However, the cost-effective, large-scale continuous preparation of graphene aerogels remains a great challenge for researchers. As is known, the traditional ice template or hydrogel-formation method requires freeze-drying machines, which could only prepare aerogels of centimeters. The CVD method may be able to achieve large-area

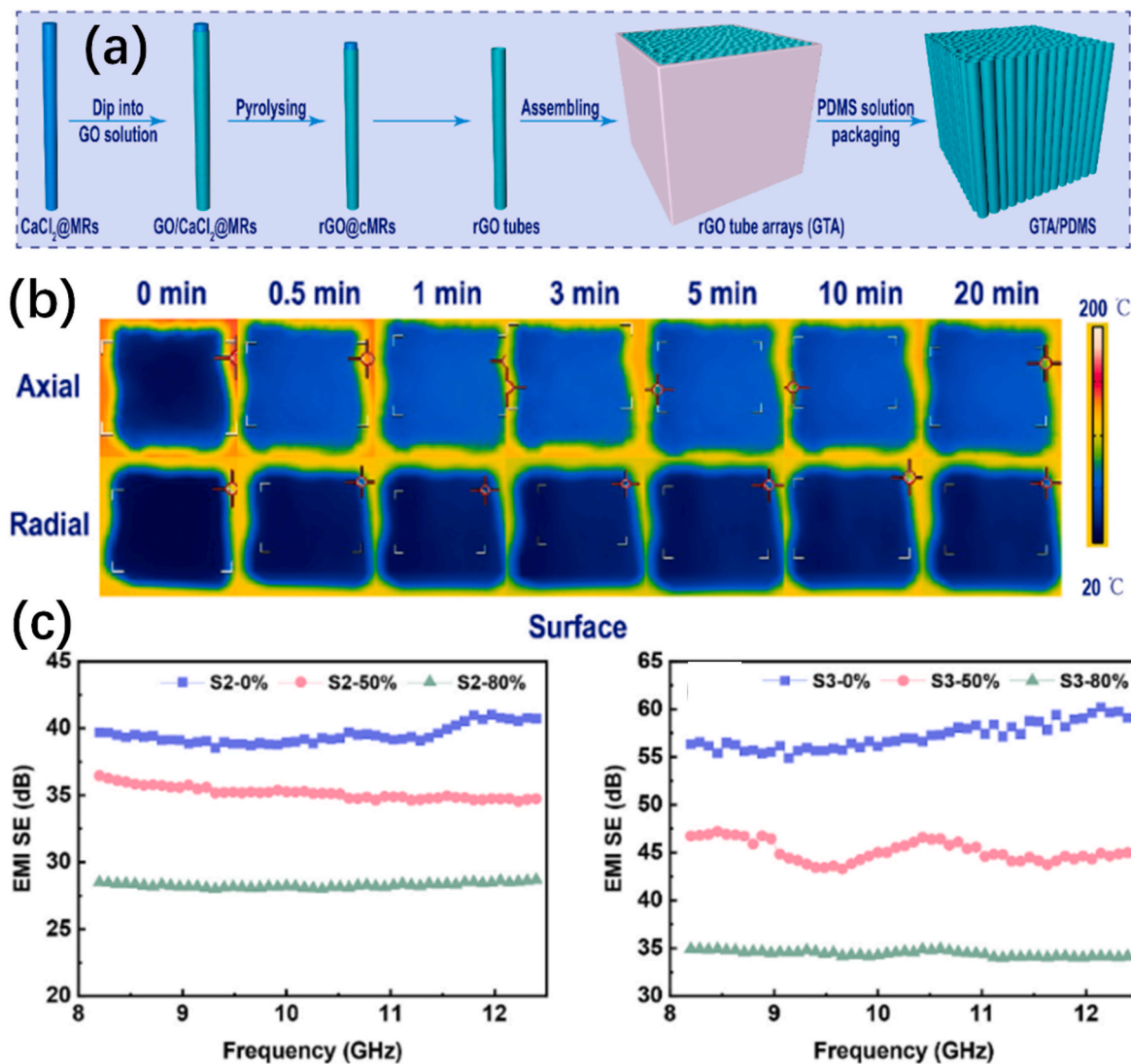


Fig. 18. (a) Schematic of the fabrication of anisotropic Graphene/PDMS composites; (b) infrared thermal images of the top surface at different times, heat transfer in the axial or radial direction; (c) EMI shielding performance of composites with different compression strains. Reprinted with permission from Ref. [177].

fabrication, but the required ambient temperature is as high as thousands of degrees Celsius, which makes it energy-intensive and complex. Therefore, further research and exploration are needed to achieve the large-scale, cost-effective preparation of graphene aerogel for practical applications.

As for the EMI shielding properties, great progress has been made by researchers, in which the best shielding performance reported has even exceeded 100 dB. However, the theoretical understanding of its EMI shielding mechanism, especially the quantitative understanding of structure/property relationships, is still lack of depth, especially how electromagnetic waves are dissipated at the molecular level of graphene sheets. How to quantify the proportion of multiple reflection/scattering contribution to EMI SE value? How is the electromagnetic energy transformed? The detailed evidences for these EMI shielding mechanisms are still lacking, and this further hinders the development of graphene aerogel as EM functional devices/equipment.

For practical applications, there are three main research directions for EMI shielding materials that should be highly noted. The first is the development of multi-band compatible EMI shielding materials. Materials that could shield wide-band EM waves are highly required in both civil and military fields. For example, the application of future 6G communication technology would require EMI shielding materials with simultaneously GHz and THz shielding performance, and the military

satellite requires EMI shielding materials with both microwaves and lasers shielding properties. Therefore, such multiband-compatible EMI shielding materials should be encouraged for further research. Secondly, the environment durability needs special attention for EMI shielding materials, since EMI shielding materials may serve in various harsh environment in the future. For instance, vessels and ships demand anti-corrosion EMI shielding materials; spacecrafts require high/low temperature-resistant EMI shielding materials. Such harsh environment may destroy the chemical/physical structure of graphene aerogel (such as oxidation in high temperature), and finally leads to weakened EMI shielding performance. So, the harsh environment-durability should be improved for future graphene aerogel-based EMI shielding materials. Thirdly, the mechanical performance of graphene aerogel should be improved for its actual application. In the past decades, many efforts have been made to fabricate graphene aerogels with elasticity and compressibility to meet various requirement. However, new strategies are still required to design the high elastic graphene aerogels by the rational design of its multiscale structure, including optimizing graphene sheets properties, selecting suitable hybrid components and designing rational nano-micro structures.

Smart EMI-shielding materials can adjust their EMI shielding performance under outer stimuli, such as voltage, temperature, laser, mechanical deformation, and magnetic field, which is a future trend of EM

functional materials and can meet the requirement of complex application conditions. Till now, the developed regulation method for materials' EMI shielding performance could be categorized into the following two aspects, including the in-situ changes of materials structure at the molecular/atomic level (such as phase change), the in-situ change of materials nano-micro structure/morphology (such as the compression of graphene foam). Based on those technologies, a large adjustable range has been achieved with Δ EMI SE value above 20 dB. Nevertheless, the exploit of intelligent electromagnetic shielding materials is still in its fancy, and various smart performances such as off/on switchable performance, and real-time frequency-adjustable performance, are immature, and new technologies/solutions should be invented. This would finally promote its application in smart wearable products, smart radar domes and smart skinning for stealth aircraft/satellites.

Declaration of competing interest

The authors declare that they have no known competing financial interests or personal relationships that could have appeared to influence the work reported in this paper.

Data availability

Data will be made available on request.

Acknowledgement

The authors gratefully acknowledge financial support from National Key R&D Program of China (MoST 2019YFA0705900, 2020YFA0711500), the National Natural Science Foundation of China (NSFC, 21875114, 21935007), 111 project (B18030) and "The Fundamental Research Funds for the Central Universities", Nankai University.

References

- [1] Q. Zhang, Z. Du, M. Hou, Z. Ding, X. Huang, A. Chen, Y. Ma, S. Lu, X.-Z. Tang, Ultralight, anisotropic, and self-supported graphene/MWCNT aerogel with high-performance microwave absorption, *Carbon* 188 (2022) 442–452.
- [2] H. Won, Y.-K. Hong, M. Choi, H. Garcia, D. Shin, Y.-S. Yoon, K. Lee, H. Xin, C.-D. Yeo, Microwave absorption performance of M-type hexagonal ferrite and MXene composite in Ka and V bands (5G mmWave frequency bands), *J. Magn. Mater.* 560 (2022), 169523.
- [3] Y. Stein, I.G. Udasin, Electromagnetic hypersensitivity (EHS, microwave syndrome)—Review of mechanisms, *Environ. Res.* 186 (2020), 109445.
- [4] W. Chongchitpaisan, P. Wiwatanadate, S. Tanprawate, A. Narkpongphan, N. Siripon, New trend of headaches among high school students affected by smartphone electromagnetic pollution exposures: a time series study, *Am. J. Publ. Health* 7 (4) (2019) 161–166.
- [5] H. Liu, R. Fu, X. Su, B. Wu, H. Wang, Y. Xu, X. Liu, MXene confined in shape-stabilized phase change material combining enhanced electromagnetic interference shielding and thermal management capability, *Compos. Sci. Technol.* 210 (2021), 108835.
- [6] Y. Cao, Z. Zeng, D. Huang, Y. Chen, L. Zhang, X. Sheng, Multifunctional phase change composites based on biomass/MXene-derived hybrid scaffolds for excellent electromagnetic interference shielding and superior solar/electro-thermal energy storage, *Nano Res.* 15 (9) (2022) 8524–8535.
- [7] M. Zhou, J. Wang, Y. Zhao, G. Wang, W. Gu, G. Ji, Hierarchically porous wood-derived carbon scaffold embedded phase change materials for integrated thermal energy management, electromagnetic interference shielding and multifunctional application, *Carbon* 183 (2021) 515–524.
- [8] H. Liu, S. Wu, C. You, N. Tian, Y. Li, N. Chopra, Recent progress in morphological engineering of carbon materials for electromagnetic interference shielding, *Carbon* 172 (2021) 569–596.
- [9] S. Singh, P. Tripathi, A. Bhatnagar, C.R.P. Patel, A.P. Singh, S. Dhawan, B. K. Gupta, O. Srivastava, A highly porous, light weight 3D sponge like graphene aerogel for electromagnetic interference shielding applications, *RSC Adv.* 5 (129) (2015) 107083–107087.
- [10] H. Nallabothula, Y. Bhattacharjee, L. Samantara, S. Bose, Processing-mediated different states of dispersion of multiwalled carbon nanotubes in PDMS nanocomposites influence EMI shielding performance, *ACS Omega* 4 (1) (2019) 1781–1790.
- [11] C.-B. Li, Y.-J. Li, Q. Zhao, Y. Luo, G.-Y. Yang, Y. Hu, J.-J. Jiang, Electromagnetic interference shielding of graphene aerogel with layered microstructure fabricated via mechanical compression, *ACS Appl. Mater. Interfaces* 12 (27) (2020) 30686–30694.
- [12] J. Xi, Y. Li, E. Zhou, Y. Liu, W. Gao, Y. Guo, J. Ying, Z. Chen, G. Chen, C. Gao, Graphene aerogel films with expansion enhancement effect of high-performance electromagnetic interference shielding, *Carbon* 135 (2018) 44–51.
- [13] L.-C. Jia, D.-X. Yan, X. Liu, R. Ma, H.-Y. Wu, Z.-M. Li, Highly efficient and reliable transparent electromagnetic interference shielding film, *ACS Appl. Mater. Interfaces* 10 (14) (2018) 11941–11949.
- [14] Q. Wei, S. Pei, X. Qian, H. Liu, Z. Liu, W. Zhang, T. Zhou, Z. Zhang, X. Zhang, H. M. Cheng, Superhigh electromagnetic interference shielding of ultrathin aligned pristine graphene nanosheets film, *Adv. Mater.* 32 (14) (2020), 1907411.
- [15] M. Zhang, P. Zhang, Q. Wang, L. Li, S. Dong, J. Liu, W. Rao, Stretchable liquid metal electromagnetic interference shielding materials with superior effectiveness, *J. Mater. Chem. C* 7 (33) (2019) 10331–10337.
- [16] C.M. Koo, P. Sambyal, A. Iqbal, F. Shahzad, J. Hong, Two-Dimensional Materials for Electromagnetic Shielding, *John Wiley & Sons* 2021.
- [17] F. Shahzad, M. Alhabeb, C.B. Hatter, B. Anasori, S. Man Hong, C.M. Koo, Y. Gogotsi, Electromagnetic interference shielding with 2D transition metal carbides (MXenes), *Science* 353 (6304) (2016) 1137–1140.
- [18] Z. Zeng, F. Jiang, Y. Yue, D. Han, L. Lin, S. Zhao, Y.B. Zhao, Z. Pan, C. Li, G. Nyström, Flexible and ultrathin waterproof cellular membranes based on high-conjunction metal-wrapped polymer nanofibers for electromagnetic interference shielding, *Adv. Mater.* 32 (19) (2020), 1908496.
- [19] H. Duan, P. He, H. Zhu, Y. Yang, G. Zhao, Y. Liu, Constructing 3D carbon-metal hybrid conductive network in polymer for ultra-efficient electromagnetic interference shielding, *Compos. B Eng.* 212 (2021), 108690.
- [20] S.H. Ryu, Y.K. Han, S.J. Kwon, T. Kim, B.M. Jung, S.-B. Lee, B. Park, Absorption-dominant, low reflection EMI shielding materials with integrated metal mesh/TPU/CIP composite, *Chem. Eng. J.* 428 (2022), 131167.
- [21] Y. Han, Y. Liu, L. Han, J. Lin, P. Jin, High-performance hierarchical graphene/metal-mesh film for optically transparent electromagnetic interference shielding, *Carbon* 115 (2017) 34–42.
- [22] S. Gupta, N.-H. Tai, Carbon materials and their composites for electromagnetic interference shielding effectiveness in X-band, *Carbon* 152 (2019) 159–187.
- [23] R. Kumar, S. Sahoo, E. Joanni, R.K. Singh, W.K. Tan, K.K. Kar, A. Matsuda, Recent progress on carbon-based composite materials for microwave electromagnetic interference shielding, *Carbon* 177 (2021) 304–331.
- [24] N. Wu, Q. Hu, R. Wei, X. Mai, N. Naik, D. Pan, Z. Guo, Z. Shi, Review on the electromagnetic interference shielding properties of carbon based materials and their novel composites: recent progress, challenges and prospects, *Carbon* 176 (2021) 88–105.
- [25] W. Zhang, L. Wei, Z. Ma, Q. Fan, J. Ma, Advances in waterborne polymer/carbon material composites for electromagnetic interference shielding, *Carbon* 177 (2021) 412–426.
- [26] B. Zhou, G. Han, Z. Zhang, Z. Li, Y. Feng, J. Ma, C. Liu, C. Shen, Aramid nanofiber-derived carbon aerogel film with skin-core structure for high electromagnetic interference shielding and solar-thermal conversion, *Carbon* 184 (2021) 562–570.
- [27] J. Kim, G. Kim, S.-Y. Kim, S. Lee, Y. Kim, J. Lee, J. Kim, Y.C. Jung, J. Kwon, H. Han, Fabrication of highly flexible electromagnetic interference shielding polyimide carbon black composite using hot-pressing method, *Compos. B Eng.* 221 (2021), 109010.
- [28] R. Zhu, Z. Li, G. Deng, Y. Yu, J. Shui, R. Yu, C. Pan, X. Liu, Anisotropic magnetic liquid metal film for wearable wireless electromagnetic sensing and smart electromagnetic interference shielding, *Nano Energy* 92 (2022), 106700.
- [29] L. Ma, M. Hamidinejad, B. Zhao, C. Liang, C.B. Park, Layered foam/film polymer nanocomposites with highly efficient EMI shielding properties and ultralow reflection, *Nano-Micro Lett.* 14 (1) (2022) 1–18.
- [30] J. Yang, Y. Chen, B. Wang, Y. Zhou, X. Chai, X. Yan, W. Han, C. Liu, P. Lin, Y. Xia, Gradient structure silicone rubber composites for selective electromagnetic interference shielding enhancement and low reflection, *Compos. Sci. Technol.* 229 (2022), 109688.
- [31] W.-C. Yu, T. Wang, Y.-H. Liu, Z.-G. Wang, L. Xu, J.-H. Tang, K. Dai, H.-J. Duan, J.-Z. Xu, Z.-M. Li, Superior and highly absorbed electromagnetic interference shielding performance achieved by designing the reflection-absorption-integrated shielding compartment with conductive wall and lossy core, *Chem. Eng. J.* 393 (2020), 124644.
- [32] H. Duan, H. Zhu, J. Gao, D.-X. Yan, K. Dai, Y. Yang, G. Zhao, Y. Liu, Z.-M. Li, Asymmetric conductive polymer composite foam for absorption dominated ultra-efficient electromagnetic interference shielding with extremely low reflection characteristics, *J. Mater. Chem. B* 8 (18) (2020) 9146–9159.
- [33] B. Shen, Y. Li, D. Yi, W. Zhai, X. Wei, W. Zheng, Microcellular graphene foam for improved broadband electromagnetic interference shielding, *Carbon* 102 (2016) 154–160.
- [34] Y. Wu, Z. Wang, X. Liu, X. Shen, Q. Zheng, Q. Xue, J.-K. Kim, Ultralight graphene foam/conductive polymer composites for exceptional electromagnetic interference shielding, *ACS Appl. Mater. Interfaces* 9 (10) (2017) 9059–9069.
- [35] L. Wang, Y. Wu, Y. Wang, H. Li, N. Jiang, K. Niu, Laterally compressed graphene foam/acrylonitrile butadiene styrene composites for electromagnetic interference shielding, *Compos. Appl. Sci. Manuf.* 133 (2020), 105887.
- [36] H. Liu, Y. Xu, X. Zhao, D. Han, F. Zhao, Q. Yang, Lightweight leaf-structured carbon nanotubes/graphene foam and the composites with polydimethylsiloxane for electromagnetic interference shielding, *Carbon* 191 (2022) 183–194.
- [37] M. Li, F. Han, S. Jiang, M. Zhang, Q. Xu, J. Zhu, A. Ge, L. Liu, Lightweight cellulose nanofibril/reduced graphene oxide aerogels with unidirectional pores

- for efficient electromagnetic interference shielding, *Adv. Mater. Interfac.* 8 (24) (2021), 2101437.
- [38] H. Guo, T. Hua, J. Qin, Q. Wu, R. Wang, B. Qian, L. Li, X. Shi, A New Strategy of 3D Printing Lightweight Lamellar Graphene Aerogels for Electromagnetic Interference Shielding and Piezoresistive Sensor Applications, *Advanced Materials Technologies*, 2022, 2101699.
- [39] X.-H. Li, X. Li, K.-N. Liao, P. Min, T. Liu, A. Dasari, Z.-Z. Yu, Thermally annealed anisotropic graphene aerogels and their electrically conductive epoxy composites with excellent electromagnetic interference shielding efficiencies, *ACS Appl. Mater. Interfaces* 8 (48) (2016) 33230–33239.
- [40] X. Wu, G. Hong, X. Zhang, Electroless plating of graphene aerogel fibers for electrothermal and electromagnetic applications, *Langmuir* 35 (10) (2019) 3814–3821.
- [41] Y.-J. Wan, P.-L. Zhu, S.-H. Yu, R. Sun, C.-P. Wong, W.-H. Liao, Ultralight, super-elastic and volume-preserving cellulose fiber/graphene aerogel for high-performance electromagnetic interference shielding, *Carbon* 115 (2017) 629–639.
- [42] Y.-Y. Wang, W.-J. Sun, D.-X. Yan, K. Dai, Z.-M. Li, Ultralight carbon nanotube/graphene/polyimide foam with heterogeneous interfaces for efficient electromagnetic interference shielding and electromagnetic wave absorption, *Carbon* 176 (2021) 118–125.
- [43] S. Bi, L. Zhang, C. Mu, M. Liu, X. Hu, Electromagnetic interference shielding properties and mechanisms of chemically reduced graphene aerogels, *Appl. Surf. Sci.* 412 (2017) 529–536.
- [44] T. Li, D. Zhi, Y. Chen, B. Li, Z. Zhou, F. Meng, Multiaxial electrospun generation of hollow graphene aerogel spheres for broadband high-performance microwave absorption, *Nano Res.* 13 (2) (2020) 477–484.
- [45] X. Huang, G. Yu, Y. Zhang, M. Zhang, G. Shao, Design of cellular structure of graphene aerogels for electromagnetic wave absorption, *Chem. Eng. J.* 426 (2021), 131894.
- [46] Z. Wang, R. Wei, J. Gu, H. Liu, C. Liu, C. Luo, J. Kong, Q. Shao, N. Wang, Z. Guo, Ultralight, Highly compressible and fire-retardant graphene aerogel with self-adjustable electromagnetic wave absorption, *Carbon* 139 (2018) 1126–1135.
- [47] Y. Cheng, K. Wang, Y. Qi, Z. Liu, Chemical vapor deposition method for graphene fiber materials, *Acta Phys. Chim. Sin.* 38 (2022), 2006046.
- [48] B. Fang, D. Chang, Z. Xu, C. Gao, A review on graphene fibers: expectations, advances, and prospects, *Adv. Mater.* 32 (5) (2020), 1902664.
- [49] F. Wang, Z. Chen, J. Yang, H. Li, J. Shan, F. Zhang, B. Guan, Z. Liu, Heating characteristics of graphene glass transparent films, *Acta Phys. Chim. Sin.* 37 (10) (2021), 2001024-0.
- [50] H. Fu, Z. Yang, Y. Zhang, M. Zhu, Y. Jia, Z. Chao, D. Hu, Q. Li, SWCNT-modulated folding-resistant sandwich-structured graphene film for high-performance electromagnetic interference shielding, *Carbon* 162 (2020) 490–496.
- [51] B. Zhao, Y. Li, H. Ji, P. Bai, S. Wang, B. Fan, X. Guo, R. Zhang, Lightweight graphene aerogels by decoration of 1D CoNi chains and CNTs to achieve ultra-wide microwave absorption, *Carbon* 176 (2021) 411–420.
- [52] N. Li, L. Yang, D. Wang, C. Tang, W. Deng, Z. Wang, High-capacity amidoxime-functionalized β -cyclodextrin/graphene aerogel for selective uranium capture, *Environ. Sci. Technol.* 55 (13) (2021) 9181–9188.
- [53] H. Huang, P. Chen, X. Zhang, Y. Lu, W. Zhan, Edge-to-edge assembled graphene oxide aerogels with outstanding mechanical performance and superhigh chemical activity, *Small* 9 (8) (2013) 1397–1404.
- [54] X. Yao, W. Yu, X. Xu, F. Chen, Q. Fu, Amphiphilic, ultralight, and multifunctional graphene/nanofibrillated cellulose aerogel achieved by cation-induced gelation and chemical reduction, *Nanoscale* 7 (9) (2015) 3959–3964.
- [55] Y. Xu, X. Huang, Z. Lin, X. Zhong, Y. Huang, X. Duan, One-step strategy to graphene/Ni(OH)₂ composite hydrogels as advanced three-dimensional supercapacitor electrode materials, *Nano Res.* 6 (1) (2013) 65–76.
- [56] W. Wan, F. Zhang, S. Yu, R. Zhang, Y. Zhou, Hydrothermal formation of graphene aerogel for oil sorption: the role of reducing agent, reaction time and temperature, *New J. Chem.* 40 (4) (2016) 3040–3046.
- [57] H. Yin, C. Zhang, F. Liu, Y. Hou, Hybrid of iron nitride and nitrogen-doped graphene aerogel as synergistic catalyst for oxygen reduction reaction, *Adv. Funct. Mater.* 24 (20) (2014) 2930–2937.
- [58] H. Ren, X. Shi, J. Zhu, Y. Zhang, Y. Bi, L. Zhang, Facile synthesis of N-doped graphene aerogel and its application for organic solvent adsorption, *J. Mater. Sci.* 51 (13) (2016) 6419–6427.
- [59] J. Wang, X. Duan, Q. Dong, F. Meng, X. Tan, S. Liu, S. Wang, Facile synthesis of N-doped 3D graphene aerogel and its excellent performance in catalytic degradation of antibiotic contaminants in water, *Carbon* 144 (2019) 781–790.
- [60] Y. Zhang, H. Tao, H. Ma, S. Du, T. Li, Y. Zhang, J. Li, X. Yang, Three-dimensional MoO₂@ few-layered MoS₂ covered by S-doped graphene aerogel for enhanced lithium ion storage, *Electrochim. Acta* 283 (2018) 619–627.
- [61] L. Zhao, B. Yu, F. Xue, J. Xie, X. Zhang, R. Wu, R. Wang, Z. Hu, S.-T. Yang, J. Luo, Facile hydrothermal preparation of recyclable S-doped graphene sponge for Cu²⁺ adsorption, *J. Hazard Mater.* 286 (2015) 449–456.
- [62] X. Gao, B. Wang, Y. Zhang, H. Liu, H. Liu, H. Wu, S. Dou, Graphene-scroll-sheathed α -MnS coaxial nanocables embedded in N, S Co-doped graphene foam as 3D hierarchically ordered electrodes for enhanced lithium storage, *Energy Storage Mater.* 16 (2019) 46–55.
- [63] D. Liu, Q. Li, S. Li, J. Hou, H. Zhao, A confinement strategy to prepare N-doped reduced graphene oxide foams with desired monolithic structures for supercapacitors, *Nanoscale* 11 (10) (2019) 4362–4368.
- [64] H.-L. Guo, P. Su, X. Kang, S.-K. Ning, Synthesis and characterization of nitrogen-doped graphene hydrogels by hydrothermal route with urea as reducing-doping agents, *J. Mater. Chem.* 1 (6) (2013) 2248–2255.
- [65] Y. Li, W. Cui, L. Liu, R. Zong, W. Yao, Y. Liang, Y. Zhu, Removal of Cr(VI) by 3D TiO₂-graphene hydrogel via adsorption enriched with photocatalytic reduction, *Appl. Catal. B Environ.* 199 (2016) 412–423.
- [66] W. Chen, L. Yan, In situ self-assembly of mild chemical reduction graphene for three-dimensional architectures, *Nanoscale* 3 (8) (2011) 3132–3137.
- [67] A. Wang, S. Bok, R. Thiruvengadathan, K. Gangopadhyay, J.A. McFarland, M. R. Maschmann, S. Gangopadhyay, Reactive nanoenergetic graphene aerogel synthesized by one-step chemical reduction, *Combust. Flame* 196 (2018) 400–406.
- [68] M. Yang, N. Zhao, Y. Cui, W. Gao, Q. Zhao, C. Gao, H. Bai, T. Xie, Biomimetic architected graphene aerogel with exceptional strength and resilience, *ACS Nano* 11 (7) (2017) 6817–6824.
- [69] P. Liu, X. Li, X. Chang, P. Min, C. Shu, Y. Li, Y. Kang, Z.-Z. Yu, Highly anisotropic graphene aerogels fabricated by calcium ion-assisted unidirectional freezing for highly sensitive sensors and efficient cleanup of crude oil spills, *Carbon* 178 (2021) 301–309.
- [70] C. Yang, X. Zhu, X. Wang, J. Wang, H. Huang, Phase-field model of graphene aerogel formation by ice template method, *Appl. Phys. Lett.* 115 (11) (2019), 111901.
- [71] X. Cao, Y. Shi, W. Shi, G. Lu, X. Huang, Q. Yan, Q. Zhang, H. Zhang, Preparation of novel 3D graphene networks for supercapacitor applications, *Small* 7 (22) (2011) 3163–3168.
- [72] X. Xu, C. Guan, L. Xu, Y.H. Tan, D. Zhang, Y. Wang, H. Zhang, D.J. Blackwood, J. Wang, M. Li, Three dimensionally free-formable graphene foam with designed structures for energy and environmental applications, *ACS Nano* 14 (1) (2019) 937–947.
- [73] Y. Xue, D. Yu, L. Dai, R. Wang, D. Li, A. Roy, F. Lu, H. Chen, Y. Liu, J. Qu, B. Three-dimensional, N-doped graphene foam as a metal-free catalyst for oxygen reduction reaction, *Phys. Chem. Chem. Phys.* 15 (29) (2013) 12220–12226.
- [74] X. Du, H.-Y. Liu, Y.-W. Mai, Ultrafast synthesis of multifunctional N-doped graphene foam in an ethanol flame, *ACS Nano* 10 (1) (2016) 453–462.
- [75] R. Mo, D. Rooney, K. Sun, H.Y. Yang, 3D nitrogen-doped graphene foam with encapsulated germanium/nitrogen-doped graphene yolk-shell nanoarchitecture for high-performance flexible Li-ion battery, *Nat. Commun.* 8 (1) (2017) 1–9.
- [76] S. Ullah, M. Hasan, H.Q. Ta, L. Zhao, Q. Shi, L. Fu, J. Choi, R. Yang, Z. Liu, M. H. Rummeli, Synthesis of doped porous 3D graphene structures by chemical vapor deposition and its applications, *Adv. Funct. Mater.* 29 (48) (2019), 1904457.
- [77] K. Pang, X. Song, Z. Xu, X. Liu, Y. Liu, L. Zhong, Y. Peng, J. Wang, J. Zhou, F. Meng, Hydroplastic foaming of graphene aerogels and artificially intelligent tactile sensors, *Sci. Adv.* 6 (46) (2020), eabd4045.
- [78] X. Liu, K. Pang, H. Qin, Y. Liu, Y. Liu, C. Gao, Z. Xu, Hyperbolic graphene framework with optimum efficiency for conductive composites, *ACS Nano* 16 (9) (2022) 14703–14712.
- [79] F. Guo, Y. Wang, Y. Jiang, Z. Li, Z. Xu, X. Zhao, T. Guo, W. Jiang, C. Gao, Hydroplastic micromolding of 2D sheets, *Adv. Mater.* 33 (25) (2021), 2008116.
- [80] E. Zhu, K. Pang, Y. Chen, S. Liu, X. Liu, Z. Xu, Y. Liu, C. Gao, Ultra-stable graphene aerogels for electromagnetic interference shielding, *Science China Materials* (2022) 1–8.
- [81] Z. Chen, C. Xu, C. Ma, W. Ren, H.M. Cheng, Lightweight and flexible graphene foam composites for high-performance electromagnetic interference shielding, *Adv. Mater.* 25 (9) (2013) 1296–1300.
- [82] Y. Zhang, Y. Huang, T. Zhang, H. Chang, P. Xiao, H. Chen, Z. Huang, Y. Chen, Broadband and tunable high-performance microwave absorption of an ultralight and highly compressible graphene foam, *Adv. Mater.* 27 (12) (2015) 2049–2053.
- [83] Z. Huang, H. Chen, Y. Huang, Z. Ge, Y. Zhou, Y. Yang, P. Xiao, J. Liang, T. Zhang, Q. Shi, Ultra-broadband wide-angle terahertz absorption properties of 3D graphene foam, *Adv. Funct. Mater.* 28 (2) (2018), 1704363.
- [84] P. Liu, S. Gao, C. Chen, F. Zhou, Z. Meng, Y. Huang, Y. Wang, Vacancies-engineered and heteroatoms-regulated N-doped porous carbon aerogel for ultrahigh microwave absorption, *Carbon* 169 (2020) 276–287.
- [85] P. Liu, S. Gao, Y. Wang, F. Zhou, Y. Huang, J. Luo, Metal-organic polymer coordination materials derived Co/N-doped porous carbon composites for frequency-selective microwave absorption, *Compos. B Eng.* 202 (2020), 108406.
- [86] W. Huang, X. Zhang, Y. Zhao, J. Zhang, P. Liu, Hollow N-doped carbon polyhedra embedded Co and Mo₂C nanoparticles for high-efficiency and wideband microwave absorption, *Carbon* 167 (2020) 19–30.
- [87] J. Zhou, Y.J. Chen, H. Li, R. Dugani, Q. Du, H. UrRehman, H.M. Kang, H.Z. Liu, Facile synthesis of three-dimensional lightweight nitrogen-doped graphene aerogel with excellent electromagnetic wave absorption properties, *J. Mater. Sci.* 53 (6) (2018) 4067–4077.
- [88] P. Liu, Y. Zhang, J. Yan, Y. Huang, L. Xia, Z. Guang, Synthesis of lightweight N-doped graphene foams with open reticular structure for high-efficiency electromagnetic wave absorption, *Chem. Eng. J.* 368 (2019) 285–298.
- [89] Q. Liu, X. He, C. Yi, D. Sun, J. Chen, D. Wang, K. Liu, M. Li, Fabrication of ultralight nickel/graphene composite foam with 3D interpenetrating network for high-performance electromagnetic interference shielding, *Compos. B Eng.* 182 (2020), 107614.
- [90] Q. Gao, G. Zhang, Y. Zhang, X. Fan, Z. Wang, S. Zhang, R. Xiao, F. Huang, X. Shi, J. Qin, Absorption dominated high-performance electromagnetic interference shielding epoxy/functionalized reduced graphene oxide/Ni-chains microcellular foam with asymmetric conductive structure, *Compos. Sci. Technol.* 223 (2022), 109419.
- [91] C. Liang, P. Song, H. Qiu, Y. Zhang, X. Ma, F. Qi, H. Gu, J. Kong, D. Cao, J. Gu, Constructing interconnected spherical hollow conductive networks in silver platelets/reduced graphene oxide foam/epoxy nanocomposites for superior

- electromagnetic interference shielding effectiveness, *Nanoscale* 11 (46) (2019) 22590–22598.
- [92] Q. Gao, J. Qin, B. Guo, X. Fan, F. Wang, Y. Zhang, R. Xiao, F. Huang, X. Shi, G. Zhang, High-performance electromagnetic interference shielding epoxy/Ag nanowire/thermally annealed graphene aerogel composite with bicontinuous three-dimensional conductive skeleton, *Compos. Appl. Sci. Manuf.* 151 (2021), 106648.
- [93] X.T. Yang, S.G. Fan, Y. Li, Y.Q. Guo, Y.G. Li, K.P. Ruan, S.M. Zhang, J.L. Zhang, J. Kong, J.W. Gu, Synchronously improved electromagnetic interference shielding and thermal conductivity for epoxy nanocomposites by constructing 3D copper nanowires/thermally annealed graphene aerogel framework, *Compos. Appl. Sci. Manuf.* 128 (2020).
- [94] H. Fang, H. Guo, Y. Hu, Y. Ren, P.-C. Hsu, S.-L. Bai, In-situ grown hollow Fe₃O₄ onto graphene foam nanocomposites with high EMI shielding effectiveness and thermal conductivity, *Compos. Sci. Technol.* 188 (2020), 107975.
- [95] S. Zhu, Q. Cheng, C. Yu, X. Pan, X. Zuo, J. Liu, M. Chen, W. Li, Q. Li, L. Liu, Flexible Fe₃O₄/graphene foam/poly dimethylsiloxane composite for high-performance electromagnetic interference shielding, *Compos. Sci. Technol.* 189 (2020), 108012.
- [96] Y.M. Huangfu, C.B. Liang, Y.X. Han, H. Qiu, P. Song, L. Wang, J. Kong, J.W. Gu, Fabrication and investigation on the Fe₃O₄/thermally annealed graphene aerogel/epoxy electromagnetic interference shielding nanocomposites, *Compos. Sci. Technol.* 169 (2019) 70–75.
- [97] H. Luo, Y. Lu, J. Qiu, Double negative electromagnetic behavior and electromagnetic shielding performance of sandwich-like buckypaper/yttrium iron garnet-graphene aerogel/buckypaper metacomposites, *Carbon* 183 (2021) 34–41.
- [98] R.W. Shu, J.B. Zhang, Y. Wu, Z.L. Wan, X.H. Li, Synthesis of nitrogen-doped reduced graphene oxide/cobalt-zinc ferrite composite aerogels with superior compression recovery and electromagnetic wave absorption performance, *Nanoscale* 13 (8) (2021) 4485–4495.
- [99] X. Wang, Y. Lu, T. Zhu, S. Chang, W. Wang, CoFe₂O₄/N-doped reduced graphene oxide aerogels for high-performance microwave absorption, *Chem. Eng. J.* 388 (2020), 124317.
- [100] X.H. Ru, H.Y. Li, Y.W. Peng, Z.W. Fan, J.J. Feng, L. Gong, Z.G. Liu, Y.H. Chen, Q. Y. Zhang, A new trial for lightweight MXene hybrid aerogels with high electromagnetic interference shielding performance, *J. Mater. Sci. Mater. Electron.* 33 (7) (2022) 4093–4103.
- [101] X. Lin, P. Liu, W. Xin, Y. Teng, J. Chen, Y. Wu, Y. Zhao, X.Y. Kong, L. Jiang, L. Wen, Heterogeneous MXene/PS-b-P2VP nanofluidic membranes with controllable ion transport for osmotic energy conversion, *Adv. Funct. Mater.* 31 (45) (2021), 2105013.
- [102] J. Shen, G. Liu, Y. Ji, Q. Liu, L. Cheng, K. Guan, M. Zhang, G. Liu, J. Xiong, J. Yang, 2D MXene nanofilms with tunable gas transport channels, *Adv. Funct. Mater.* 28 (31) (2018), 1801511.
- [103] S. Zhao, H.-B. Zhang, J.-Q. Luo, Q.-W. Wang, B. Xu, S. Hong, Z.-Z. Yu, Highly electrically conductive three-dimensional Ti₃C₂T_x MXene/reduced graphene oxide hybrid aerogels with excellent electromagnetic interference shielding performances, *ACS Nano* 12 (11) (2018) 11193–11202.
- [104] W. Ma, H. Chen, S. Hou, Z. Huang, Y. Huang, S. Xu, F. Fan, Y. Chen, Compressible highly stable 3D porous MXene/GO foam with a tunable high-performance stealth property in the terahertz band, *ACS Appl. Mater. Interfaces* 11 (28) (2019) 25369–25377.
- [105] L. Jin, W. Cao, P. Wang, N. Song, P. Ding, Interconnected mxene/graphene network constructed by soft template for multi-performance improvement of polymer composites, *Nano-Micro Lett.* 14 (1) (2022) 1–17.
- [106] L.Y. Liang, Q.M. Li, X. Yan, Y.Z. Feng, Y.M. Wang, H.B. Zhang, X.P. Zhou, C.T. Liu, C.Y. Shen, X.L. Xie, Multifunctional magnetic Ti₃C₂T_x MXene/graphene aerogel with superior electromagnetic wave absorption performance, *ACS Nano* 15 (4) (2021) 6622–6632.
- [107] S.S. Li, X.W. Tang, X. Zhao, S.J. Lu, J.T. Luo, Z.Y. Chai, T.T. Ma, Q.Q. Lan, P. M. Ma, W.F. Dong, Z.C. Wang, T.X. Liu, Hierarchical graphene@MXene composite foam modified with flower-shaped FeS for efficient and broadband electromagnetic absorption, *J. Mater. Sci. Technol.* 133 (2023) 238–248.
- [108] R. Kumar, J. Trivas-Sejdic, L.P. Padhye, Conducting polymers-based photocatalysis for treatment of organic contaminants in water, *Chem. Eng. J. Adv.* 4 (2020), 100047.
- [109] S. Ghosh, N.A. Kouamé, L. Ramos, S. Remita, A. Dazzi, A. Deniset-Besseau, P. Beaunier, F. Goubard, P.-H. Aubert, H. Remita, Conducting polymer nanostructures for photocatalysis under visible light, *Nat. Mater.* 14 (5) (2015) 505–511.
- [110] A. Savateev, Y. Markushyna, C.M. Schüßlbauer, T. Ullrich, D.M. Guldi, M. Antonietti, Unconventional photocatalysis in conductive polymers: reversible modulation of PEDOT: PSS conductivity by long-lived poly (heptazine imide) radicals, *Angew. Chem. Int. Ed.* 60 (13) (2021) 7436–7443.
- [111] F. Wu, A.M. Xie, M.X. Sun, Y. Wang, M.Y. Wang, Reduced graphene oxide (RGO) modified spongelike polypyrrole (PPy) aerogel for excellent electromagnetic absorption, *J. Mater. Chem.* 3 (27) (2015) 14358–14369.
- [112] Y. Huangfu, K. Ruan, H. Qiu, Y. Lu, C. Liang, J. Kong, J. Gu, Fabrication and investigation on the PANI/MWCNT/thermally annealed graphene aerogel/epoxy electromagnetic interference shielding nanocomposites, *Compos. Appl. Sci. Manuf.* 121 (2019) 265–272.
- [113] L. Wang, H. Li, S. Xiao, M. Zhu, J. Yang, Preparation of p-phenylenediamine modified graphene foam/polyaniline@ epoxy composite with superior thermal and EMI shielding performance, *Polymers* 13 (14) (2021) 2324.
- [114] J.C. Li, X.Y. Zhao, W.J. Wu, X.W. Ji, Y.L. Lu, L.Q. Zhang, Bubble-templated rGO-graphene nanoplatelet foams encapsulated in silicon rubber for electromagnetic interference shielding and high thermal conductivity, *Chem. Eng. J.* 415 (2021).
- [115] Z. Cheng, R. Wang, Y. Cao, Z. Zhang, W. Ma, T. Zhang, F. Fan, Y. Huang, Interfacial π - π interactions induced ultralight, 300° C-stable, wideband graphene/polyaramid foam for electromagnetic wave absorption in both gigahertz and terahertz bands, *ACS Appl. Mater. Interfaces* 14 (2) (2022) 3218–3232.
- [116] Y. Fei, M. Liang, Y. Chen, H. Zou, Sandwich-like magnetic graphene papers prepared with MOF-derived Fe₃O₄-C for absorption-dominated electromagnetic interference shielding, *Ind. Eng. Chem. Res.* 59 (1) (2019) 154–165.
- [117] S.-Q. Zhu, J.-C. Shu, M.-S. Cao, Novel MOF-derived 3D hierarchical needlelike array architecture with excellent EMI shielding, thermal insulation and supercapacitor performance, *Nanoscale* 14 (19) (2022) 7322–7331.
- [118] W. Bai, J. Zhai, S. Zhou, C. Cui, W. Wang, S. Jiang, C. Cheng, E. Ren, H. Xiao, M. Zhou, Flexible MOF on CoKFel-XOOH@ biomass derived alloy@ carbon films for efficient electromagnetic interference shielding and energy conversion, *Carbon* 199 (2022) 96–109.
- [119] W. Yu, B. Liu, X. Zhao, Ultralight MOF-derived Ni₃S₂@ N, S-codoped graphene aerogels for high-performance microwave absorption, *Nanomaterials* 12 (4) (2022) 655.
- [120] S. Li, X. Tian, J. Wang, S. Xia, L. Ma, J. Zhou, C. Li, Z. Qin, S. Qu, Design and synthesis of core-shell structure 3D-graphene/Fe₃O₄@ NC composite derived from Fe-MOF as lightweight microwave absorber, *Diam. Relat. Mater.* 124 (2022), 108941.
- [121] L. Ding, Y. Huang, Z. Xu, J. Yan, X. Liu, T. Li, P. Liu, MIL-53 (Fe) derived MCC/rGO nanoparticles with excellent broadband microwave absorption properties, *Compos. Commun.* 21 (2020), 100362.
- [122] Z. Zhang, Z. Cai, L. Xia, D. Zhao, F. Fan, Y. Huang, Synergistically assembled cobalt-telluride/graphene foam with high-performance electromagnetic wave absorption in both gigahertz and terahertz band ranges, *ACS Appl. Mater. Interfaces* 13 (26) (2021) 30967–30979.
- [123] X. Huang, J. Wei, Y. Zhang, B. Qian, Q. Jia, J. Liu, X. Zhao, G. Shao, Ultralight magnetic and dielectric aerogels achieved by metal-organic framework initiated gelation of graphene oxide for enhanced microwave absorption, *Nano-Micro Lett.* 14 (1) (2022) 1–16.
- [124] P. Wang, L. Yang, J. Ling, J. Song, T. Song, X. Chen, S. Gao, S. Feng, Y. Ding, V. Murugadoss, Frontal ring-opening metathesis polymerized polydicyclopentadiene carbon nanotube/graphene aerogel composites with enhanced electromagnetic interference shielding, *Adv. Composite Hybrid Mater.* (2022) 1–12.
- [125] Z. Lu, Y. Wang, X. Di, N. Wang, R. Cheng, L. Yang, Heterostructure design of carbon fiber@ graphene@ layered double hydroxides synergistic microstructure for lightweight and flexible microwave absorption, *Carbon* 197 (2022) 466–475.
- [126] H. Lv, Y. Li, Z. Jia, L. Wang, X. Guo, B. Zhao, R. Zhang, Exceptionally porous three-dimensional architectural nanostructure derived from CNTs/graphene aerogel towards the ultra-wideband EM absorption, *Compos. B Eng.* 196 (2020), 108122.
- [127] S. Zhao, Y. Yan, A. Gao, S. Zhao, J. Cui, G. Zhang, Flexible polydimethylsilane nanocomposites enhanced with a three-dimensional graphene/carbon nanotube bicontinuous framework for high-performance electromagnetic interference shielding, *ACS Appl. Mater. Interfaces* 10 (31) (2018) 26723–26732.
- [128] H.H. Chen, Z.Y. Huang, Y. Huang, Y. Zhang, Z. Ge, B. Qin, Z.F. Liu, Q. Shi, P. S. Xiao, Y. Yang, T.F. Zhang, Y.S. Chen, Synergistically assembled MWCNT/graphene foam with highly efficient microwave absorption in both C and X bands, *Carbon* 124 (2017) 506–514.
- [129] Y. Cao, Z. Cheng, R. Wang, X. Liu, T. Zhang, F. Fan, Y. Huang, Multifunctional graphene/carbon fiber aerogels toward compatible electromagnetic wave absorption and shielding in gigahertz and terahertz bands with optimized radar cross section, *Carbon* 199 (2022) 333–346.
- [130] Y. Lin, H. Liu, C. Yang, X. Wu, C. Du, L. Jiang, Y. Zhong, Gama-graphyne as photogenerated electrons transfer layer enhances photocatalytic performance of silver phosphate, *Appl. Catal. B Environ.* 264 (2020), 118479.
- [131] A. Torres-Pinto, C.G. Silva, J.L. Faria, A.M. Silva, Advances on graphyne-family members for superior photocatalytic behavior, *Adv. Sci.* 8 (10) (2021), 2003900.
- [132] L. Wu, Q. Li, C. Yang, X. Ma, Z. Zhang, X. Cui, Constructing a novel TiO₂/γ-graphyne heterojunction for enhanced photocatalytic hydrogen evolution, *J. Mater. Chem.* 6 (42) (2018) 20947–20955.
- [133] Z. Zhang, Z. Li, L. Xia, R. Wang, Y. Cao, Z. Cheng, Y. Huang, Much enhanced electromagnetic wave absorbing properties from the synergistic effect of graphene/γ-graphyne heterostructure in both gigahertz and terahertz band ranges, *Nano Res.* 16 (2022) 88–100.
- [134] P. Song, B. Liu, C. Liang, K. Ruan, H. Qiu, Z. Ma, Y. Guo, J. Gu, Lightweight, flexible cellulose-derived carbon aerogel@ reduced graphene oxide/PDMS composites with outstanding EMI shielding performances and excellent thermal conductivities, *Nano-Micro Lett.* 13 (1) (2021) 1–17.
- [135] Z. Fan, D. Wang, Y. Yuan, Y. Wang, Z. Cheng, Y. Liu, Z. Xie, A lightweight and conductive MXene/graphene hybrid foam for superior electromagnetic interference shielding, *Chem. Eng. J.* 381 (2020), 122696.
- [136] M.-L. Wang, Z.-H. Zhou, J.-L. Zhu, H. Lin, K. Dai, H.-D. Huang, Z.-M. Li, Tunable high-performance electromagnetic interference shielding of intrinsic N-doped chitin-based carbon aerogel, *Carbon* 198 (2022) 142–150.
- [137] Z. Guo, P. Ren, J. Wang, X. Hou, J. Tang, Z. Liu, Z. Chen, Y. Jin, F. Ren, Methylene blue adsorption derived thermal insulating N, S-co-doped TiC/carbon hybrid aerogel for high-efficient absorption-dominant electromagnetic interference shielding, *Chem. Eng. J.* 451 (2023), 138667.

- [138] C. Yu, S. Zhu, C. Xing, X. Pan, X. Zuo, J. Liu, M. Chen, L. Liu, G. Tao, Q. Li, Fe nanoparticles and CNTs co-decorated porous carbon/graphene foam composite for excellent electromagnetic interference shielding performance, *J. Alloys Compd.* 820 (2020), 153108.
- [139] Q. Jiang, X. Liao, J. Yang, G. Wang, J. Chen, C. Tian, G. Li, A two-step process for the preparation of thermoplastic polyurethane/graphene aerogel composite foams with multi-stage networks for electromagnetic shielding, *Compos. Commun.* 21 (2020), 100416.
- [140] S. Gupta, S.K. Sharma, D. Pradhan, N.-H. Tai, Ultra-light 3D reduced graphene oxide aerogels decorated with cobalt ferrite and zinc oxide perform excellent electromagnetic interference shielding effectiveness, *Compos. Appl. Sci. Manuf.* 123 (2019) 232–241.
- [141] M. González, J. Baselga, J. Pozuelo, Modulating the electromagnetic shielding mechanisms by thermal treatment of high porosity graphene aerogels, *Carbon* 147 (2019) 27–34.
- [142] M.-L. Wang, S. Zhang, Z.-H. Zhou, J.-L. Zhu, J.-F. Gao, K. Dai, H.-D. Huang, Z.-M. Li, Facile heteroatom doping of biomass-derived carbon aerogels with hierarchically porous architecture and hybrid conductive network: towards high electromagnetic interference shielding effectiveness and high absorption coefficient, *Compos. B Eng.* 224 (2021), 109175.
- [143] M. Li, M. Zhang, Y. Zhao, S. Jiang, Q. Xu, F. Han, J. Zhu, L. Liu, A. Ge, Multilayer structured CNF/rGO aerogels and rGO film composites for efficient electromagnetic interference shielding, *Carbohydr. Polym.* 286 (2022), 119306.
- [144] S. Li, J. Wang, Z. Zhu, D. Liu, W. Li, G. Sui, C.B. Park, CVD carbon-coated carbonized loofah sponge loaded with a directionally arrayed MXene aerogel for electromagnetic interference shielding, *J. Mater. Chem.* 9 (1) (2021) 358–370.
- [145] H. Liu, Z. Huang, T. Chen, X. Su, Y. Liu, R. Fu, Construction of 3D MXene/Silver nanowires aerogels reinforced polymer composites for extraordinary electromagnetic interference shielding and thermal conductivity, *Chem. Eng. J.* 427 (2022), 131540.
- [146] P. He, M.-S. Cao, Y.-Z. Cai, J.-C. Shu, W.-Q. Cao, J. Yuan, Self-assembling flexible 2D carbide MXene film with tunable integrated electron migration and group relaxation toward energy storage and green EMI shielding, *Carbon* 157 (2020) 80–89.
- [147] J. Zhang, N. Kong, S. Uzun, A. Levitt, S. Seyedin, P.A. Lynch, S. Qin, M. Han, W. Yang, J. Liu, Scalable manufacturing of free-standing, strong Ti3C2Tx MXene films with outstanding conductivity, *Adv. Mater.* 32 (23) (2020), 2001093.
- [148] H. Jia, Q.-Q. Kong, X. Yang, L.-J. Xie, G.-H. Sun, L.-L. Liang, J.-P. Chen, D. Liu, Q.-G. Guo, C.-M. Chen, Dual-functional graphene/carbon nanotubes thick film: bidirectional thermal dissipation and electromagnetic shielding, *Carbon* 171 (2021) 329–340.
- [149] L. Li, Z. Ma, P. Xu, B. Zhou, Q. Li, J. Ma, C. He, Y. Feng, C. Liu, Flexible and alternant-layered cellulose nanofiber/graphene film with superior thermal conductivity and efficient electromagnetic interference shielding, *Compos. Appl. Sci. Manuf.* 139 (2020), 106134.
- [150] Y. Fang, X. Li, M. Sheng, S. Gong, H. Wu, X. Lu, J. Qu, Nickel foam encapsulated phase change composites with outstanding electromagnetic interference shielding and thermal management capability, *Compos. Appl. Sci. Manuf.* 160 (2022), 107056.
- [151] Y.J. Wan, P.L. Zhu, S.H. Yu, R. Sun, C.P. Wong, W.H. Liao, Anticorrosive, ultralight, and flexible carbon-wrapped metallic nanowire hybrid sponges for highly efficient electromagnetic interference shielding, *Small* 14 (27) (2018), 1800534.
- [152] X. Liu, Y. Li, X. Sun, W. Tang, G. Deng, Y. Liu, Z. Song, Y. Yu, R. Yu, L. Dai, Off/on switchable smart electromagnetic interference shielding aerogel, *Matter* 4 (5) (2021) 1735–1747.
- [153] B. Wen, M.-S. Cao, Z.-L. Hou, W.-L. Song, L. Zhang, M.-M. Lu, H.-B. Jin, X.-Y. Fang, W.-Z. Wang, J. Yuan, Temperature dependent microwave attenuation behavior for carbon-nanotube/silica composites, *Carbon* 65 (2013) 124–139.
- [154] W.-Q. Cao, X.-X. Wang, J. Yuan, W.-Z. Wang, M.-S. Cao, Temperature dependent microwave absorption of ultrathin graphene composites, *J. Mater. Chem. C* 3 (38) (2015) 10017–10022.
- [155] X.-Y. Fang, X.-X. Yu, H.-M. Zheng, H.-B. Jin, L. Wang, M.-S. Cao, Temperature-and thickness-dependent electrical conductivity of few-layer graphene and graphene nanosheets, *Phys. Lett.* 379 (37) (2015) 2245–2251.
- [156] M. Cao, X. Wang, W. Cao, X. Fang, B. Wen, J. Yuan, Thermally driven transport and relaxation switching self-powered electromagnetic energy conversion, *Small* 14 (29) (2018), 1800987.
- [157] B. Wen, M. Cao, M. Lu, W. Cao, H. Shi, J. Liu, X. Wang, H. Jin, X. Fang, W. Wang, Reduced graphene oxides: light-weight and high-efficiency electromagnetic interference shielding at elevated temperatures, *Adv. Mater.* 26 (21) (2014) 3484–3489.
- [158] M.-S. Cao, J.-C. Shu, B. Wen, X.-X. Wang, W.-Q. Cao, Genetic dielectric genes inside 2D carbon-based materials with tunable electromagnetic function at elevated temperature, *Small Struct.* 2 (11) (2021), 2100104.
- [159] Z. Cheng, R. Wang, Y. Cao, Z. Cai, Z. Zhang, Y. Huang, Intelligent off/on switchable microwave absorption performance of reduced graphene oxide/VO2 composite aerogel, *Adv. Funct. Mater.* (2022), 2205160.
- [160] Y. Li, D. Gao, Y. Guo, W. Wei, Y. Wang, H. Jiang, F. Peng, F. Meng, Z. Zhou, A temperature-responsive composite for adaptive microwave absorption, *Chem. Eng. J.* 427 (2022), 131746.
- [161] B. Sensale-Rodriguez, R. Yan, M.M. Kelly, T. Fang, K. Tahy, W.S. Hwang, D. Jena, L. Liu, H.G. Xing, Broadband graphene terahertz modulators enabled by intraband transitions, *Nat. Commun.* 3 (1) (2012) 1–7.
- [162] W. Lim, Y. Yap, W. Chong, C. Pua, N. Huang, R. De La Rue, H. Ahmad, Graphene oxide-based waveguide polariser: from thin film to quasi-bulk, *Opt Express* 22 (9) (2014) 11090–11098.
- [163] H. Chen, Z. Huang, Y. Huang, Y. Zhang, Z. Ge, W. Ma, T. Zhang, M. Wu, S. Xu, F. Fan, Consecutively strong absorption from gigahertz to terahertz bands of a monolithic three-dimensional Fe3O4/graphene material, *ACS Appl. Mater. Interfaces* 11 (1) (2018) 1274–1282.
- [164] S.T. Xu, F. Fan, J. Cheng, H. Chen, W. Ma, Y. Huang, S. Chang, Active terahertz shielding and absorption based on graphene foam modulated by electric and optical field excitation, *Adv. Opt. Mater.* 7 (18) (2019), 1900555.
- [165] J. Xu, H. Chang, B. Zhao, R. Li, T. Cui, J. Jian, Y. Yang, H. Tian, S. Zhang, T.-L. Ren, Highly stretchable and conformal electromagnetic interference shielding armor with strain sensing ability, *Chem. Eng. J.* 431 (2022), 133908.
- [166] C. Liang, Y. Liu, Y. Ruan, H. Qiu, P. Song, J. Kong, H. Zhang, J. Gu, Multifunctional sponges with flexible motion sensing and outstanding thermal insulation for superior electromagnetic interference shielding, *Compos. Appl. Sci. Manuf.* 139 (2020), 106143.
- [167] G. Zu, K. Kanamori, K. Nakanishi, X. Lu, K. Yu, J. Huang, H. Sugimura, Superelastic multifunctional aminosilane-crosslinked graphene aerogels for high thermal insulation, three-component separation, and strain/pressure-sensing arrays, *ACS Appl. Mater. Interfaces* 11 (46) (2019) 43533–43542.
- [168] V.-T. Nguyen, B.K. Min, Y. Yi, S.J. Kim, C.-G. Choi, MXene (Ti3C2Tx)/graphene/PDMS composites for multifunctional broadband electromagnetic interference shielding skins, *Chem. Eng. J.* 393 (2020), 124608.
- [169] J. Xu, R. Li, S. Ji, B. Zhao, T. Cui, X. Tan, G. Gou, J. Jian, H. Xu, Y. Qiao, Multifunctional graphene microstructures inspired by honeycomb for ultrahigh performance electromagnetic interference shielding and wearable applications, *ACS Nano* 15 (5) (2021) 8907–8918.
- [170] C. Li, L. Qiu, B. Zhang, D. Li, C.Y. Liu, Robust vacuum-/air-dried graphene aerogels and fast recoverable shape-memory hybrid foams, *Adv. Mater.* 28 (7) (2016) 1510–1516.
- [171] X. Cao, J. Zhang, S. Chen, R.J. Varley, K. Pan, 1D/2D nanomaterials synergistic, compressible, and response rapidly 3D graphene aerogel for piezoresistive sensor, *Adv. Funct. Mater.* 30 (35) (2020), 2003618.
- [172] F. Guo, Y. Jiang, Z. Xu, Y. Xiao, B. Fang, Y. Liu, W. Gao, P. Zhao, H. Wang, C. Gao, Highly stretchable carbon aerogels, *Nat. Commun.* 9 (1) (2018) 1–9.
- [173] Z. Zeng, C. Wang, Y. Zhang, P. Wang, S.I. Seyed Shahabadi, Y. Pei, M. Chen, X. Lu, Ultralight and highly elastic graphene/lignin-derived carbon nanocomposite aerogels with ultrahigh electromagnetic interference shielding performance, *ACS Appl. Mater. Interfaces* 10 (9) (2018) 8205–8213.
- [174] C. Wang, C. Zhang, S. Chen, Micro-mechanism and influencing factors of graphene foam elasticity, *Carbon* 148 (2019) 267–276.
- [175] J. Liu, Y. Liu, H.-B. Zhang, Y. Dai, Z. Liu, Z.-Z. Yu, Superelastic and multifunctional graphene-based aerogels by interfacial reinforcement with graphitized carbon at high temperatures, *Carbon* 132 (2018) 95–103.
- [176] X. Jiang, Z. Zhao, S. Zhou, H. Zou, P. Liu, Anisotropic and Lightweight Carbon/Graphene Composite Aerogels for Efficient Thermal Insulation and Electromagnetic Interference Shielding, *ACS Applied Materials & Interfaces*, 2022.
- [177] J. Chen, B. Shen, X. Jia, Y. Liu, W. Zheng, Lightweight and compressible anisotropic honeycomb-like graphene composites for highly tunable electromagnetic shielding with multiple functions, *Materials Today Physics* 24 (2022), 100695.